The Effect of Light Elements on Metal/ Silicate Partitioning

Submitted by Francesca J. Mirolo, St. Hugh's College

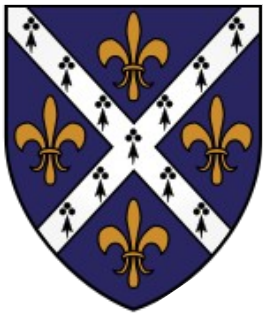

MSci Research Thesis

Department of Earth Sciences, University of Oxford

Supervised by Professor Bernard J. Wood

Oxford, 2013

I hereby declare that this thesis is my own original research and wherever contributions of others are involved, every effort is made to indicate this clearly, with due reference to the literature and acknowledgements.

Francesca Mirolo, October 2013

Table of contents

Acknowledgements

I would like to express my deep gratitude to my supervisor Dr. Bernard Wood for his guidance and expertise, which he shared generously with me during the course of this project. I would also like to thank Dr. Ekaterina Kiseeva for providing critiques and feedback for draft versions of my thesis. My grateful thanks are also extended to Dr. Jon Wade, Dr. James Tuff and Mr. Ashley Norris for extensive training within the laboratory and guidance during writing my thesis. Finally I would like to thank my friends for their care and support throughout my study.

List of Figures

List of Tables

Abstract

The accretion of the Earth was marked by the high-pressure segregation of most of its core, accompanied by dissolution of about 10% of one or more "light" elements into the metallic phase. Various light elements have been proposed including S, Si, C and O, with each having an effect on the partitioning behaviour of the trace elements. Metallurgical data indicate that dissolution of even small amounts of light elements in liquid Fe can have profound effects on the activities of some trace components. For instance, significant partitioning of Si into the core of the growing Earth should have affected the observed Mo content of the mantle (Ono-Nakazato *et al.*, 2007).

Here, I use the epsilon model of non-ideal interactions in Fe liquids (ε. I present interaction parameters (ε, derived from 1.5GPa, 1550-1650°C metal-silicate equilibration experiments, for W, Ni, Co and Mo in liquid Fe alloyed with C, and W, Ni, Co, Mo, Cu, Mn, Ag, Sb, Cd, In, Tl, Pb, Ga, Ge, Cr, V and Zn in liquid Fe alloyed with S. Additional epsilon values were taken from the steelmaking sourcebook when necessary.

I used this new data in conjunction with published metal–silicate partitioning results to develop a model of continuous accretion and core segregation taking explicit account of the partitioning of Si (this study) and O (from Ozawa et al., 2008) between metal and silicate and their effects on metal–silicate partitioning of siderophile elements. The best model for explaining the Earth's formation including the Mo:W ratio of the silicate Earth posits that the Earth's oxidation state increased in steps from 1 to 6.26% FeO, increasing Si in the Earth's core and the light elements C and S being added to the planet in the last ~20% of accretion material.

Expanded Abstract

The nature of the protoplanetary materials which formed the Earth and Mars are still poorly known despite an abundance of samples in meteorite collections. Analyses of CI chondrite meteorites revealed that they have a close compositional match to the solar photosphere, however, except for volatile H and He. Peridotite and mantle xenolith samples were shown by McDonough and Sun (1995) to have CI chondritic proportions of refractory lithophile elements, thus CI chondrites are generally used as a proxy material for the early Earth and Mars.

A key phase in the accretion of the Earth and Mars was the high-pressure segregation of their crusts and core from the mantle. The bulk compositions of the layers are unconstrained, however, given the absence of deep mantle or core samples from either planet. Earth's core is chiefly comprised of iron and nickel, although seismological data indicate that the core is not a pure iron-nickel alloy, and that its' segregation also involved the dissolution of about 10% of one or more "light" elements into the metallic phase from the original protoplanetary material. Various light elements (those of an atomic number lower than that of iron) such as S, Si, C and O have been proposed, with each one having an effect on the mantle-core partitioning behaviour of trace elements. Metallurgical data indicate that variations in temperature and pressure, and dissolution of even small amounts of light elements in liquid Fe can have profound effects on the activities of some trace components. For example, significant partitioning of Si into the core of the growing Earth should have affected the observed Mo content of the mantle (Ono-Nakazato *et al.,* 2007).

Given the profound effects of dissolved "light" elements on metal-silicate partitioning, there is a need for more experimental data on the effects of light elements on partitioning in order to build a more reliable model of planetary accretion based on elemental abundances in the mantle. The aim of this project was to determine experimentally at high pressures and temperatures the changes in siderophile behaviour of Co, Ni, Mo, W, Cu, Ag, Sb, Mn, Cd, Pb, Tl, V, Zn,

Ge and Ga caused by the addition of the important and common “light” elements, carbon and sulphur.

All experiments were based on mixtures of 50-75% metal (either pure Fe or Fe/ FeS mix) and 25-50% synthetic silicate, by weight, and then subsequently doped with a small amount of either a trace element mix, or with higher amounts of Ni, Co, Mo and W in order to obtain measurable abundances of these elements in the silicate portion of the sample. Reagent grade FeO was added to some experiments in order to adjust the oxygen fugacity to desired values. These compositions were run in MgO, graphite or silica glass capsules at high pressures and temperatures. Graphite capsules provided the material for saturating an experiment in carbon, with MgO capsules providing C-free experiments and peridotite-like silicate liquid conditions. Since polycrystalline MgO rapidly absorbs Ni and Co from samples, however, experiments using these two trace elements employed silica glass capsules. The latter appear to retain Ni and Co reasonably well.

Experiments were performed at 1.5 GPa, using an end-loaded piston-cylinder apparatus. All experiments used a half-inch $BaCO_3$-SiO_2 glass assembly with graphite heaters and MgO internal spacers. A 1mm alumina disc served to separate the type C thermocouples ($W_{95}Re_5$-$W_{74}Re_{26}$) from the sample while measuring and controlling the temperature of 1550-1635°C adequately. Experiment durations were 10-30 minutes, previously found to be suitable to achieve constant partitioning of trace elements for these conditions of capsule size, temperature and pressure (Tuff, Wood and Wade 2011; Wood and Halliday 2010). All experiments were quenched by cutting power to the graphite heaters while maintaining water flow and pressure, to be later released gently. The run products were mounted in acrylic resin and polished. Analysis was performed using a JEOL JXA8600 electron microprobe for the silicate and metal phases in the Department of Archaeology at the University of Oxford. Trace element concentrations were measured in experimental products using Laser Ablation Inductively Coupled Mass Spectrometry. Measurements were made using a Perkin Elmer Nexion quadrupole mass spectrometer coupled to a New Wave Research UP213 Nd:YAG laser at the University of Oxford.

Here, I use the epsilon model of non-ideal interactions in Fe liquids (ε). I present interaction parameters (ε, derived from 1.5GPa, 1550-1650°C metal-silicate equilibration experiments, for W, Ni, Co and Mo in liquid Fe alloyed with C, and W, Ni, Co, Mo, Cu, Mn, Ag, Sb, Cd, In, Tl, Pb, Ga, Ge, Cr, V and Zn in liquid Fe alloyed with S. Additional epsilon values were taken from the steelmaking sourcebook when necessary.

I used these new experimental data in conjunction with published metal–silicate partitioning results to develop a model of continuous accretion and core segregation taking explicit account of the partitioning of Si (this study) and O (from Ozawa et al., 2008) between metal and silicate and their effects on metal–silicate partitioning of siderophile elements. An initial model incorporating Si and O partitioning proved inadequate because, although the Ni, Co and W core-mantle partitioning matched well, the derived pressures were too high to result in the correct Mo/W ratio of the silicate Earth. A later model includes the addition of C and S (1.1% and 1.7%, respectively) in the metal component during planetary accretion, which does increases the partitioning of Mo, but not in a sufficient amount to match its abundance in the silicate Earth. The best model for explaining the Earth's formation including the observed Mo:W ratio of the silicate Earth posits that the Earth's oxidation state increased in steps from 1 to 6.26% FeO, increasing Si in the Earth's core with the light elements C and S being predominantly added to the planet in the last ~20% of accretion material.

Thesis structure

This thesis is subdivided into five chapters. Chapter 1 provides a comprehensive literature review of the earlier research into metal-silicate partitioning under a range of variables such as temperature, pressure and compositions. In this chapter, I try to set up the problems involved in determining the conditions of core formation in the Earth and Mars, to describe the state of current knowledge in the field of metal-silicate partitioning.

Chapter 1 describes what aims and tasks my project follows in order to achieve the goal of the thesis.

Chapter 2 gives an overview of the experimental methods and techniques that have been used for the purpose of this thesis. It also describes a set of analytical techniques incorporated for analysis of the samples.

Chapter 3 details the experimental results obtained from analysis of the samples and lists them in table and graph formats.

Chapter 4 discusses the implications of the results for core formation in the Earth and Mars and compares the results of this study with previous work.

Chapter 5 lists the conclusions derived from the literature and my research.

Chapter 1. Motivation and literature overview

The original building materials for the Earth and Mars are still relatively unknown, despite there being abundant samples within meteorite collections. Looking to primitive meteorites, it was found that the CI chondrites have a composition that is a close match to that of the solar photosphere, minus the volatile H and He McDonough and Sun (1995). An analysis of peridotite massif and xenolith samples revealed they have trends in the Mg vs. CaO, Al_2O_3 (wt%) Ni and Yb (ppm) ratio-ratio plots which pass through the CI chondritic values for refractory lithophile element ratios, strongly suggesting these peridotites had originally contained these refractory elements in chondritic proportions. This implies that the silicate Earth has chondritic relative abundances of the refractory lithophile elements. Hence the CI chondritic composition is used as a proxy for the early Earth and Mars (McDonough and Sun, 1995). As the two planets formed, this original material segregated into cores, mantles and crusts. However the bulk composition of each of these layers is somewhat unconstrained, given it is currently impossible to obtain a core or even a deep mantle sample from either Earth or Mars.

The conditions that the Earth and Mars formed under have been the subject of considerable interest and may, in principle, be constrained by the compositions of the primitive silicate mantles. Material in the solar nebula began as dust grains that slowly congealed into bigger masses until reaching the size of 1 km planetesimals, which then collided and grew at an increased rate, the stage of runaway growth, culminating in larger protoplanets that grow more slowly. (Kokubo and Ida, 2000). Accretion models that have been put forward can be divided into homogeneous and heterogeneous models, the former suggesting that the terrestrial planets accreted from material of constant composition which then segregated into different layers once a critical mass and internal temperature was reached (Azbel *et al.* 1993). Heterogeneous models propose that over time the compositions of materials colliding with the growing planets changed and consequently influenced their overall bulk compositions (Ertel *et al.* 2006). Currently many hybrid models are being developed, including the theory

of a late veneer adding volatiles and extra siderophile elements to the mantles of accreting planets (Li and Agee, 2001). The latter authors found that the current concentration of S in the mantle of 250 +/- 50 ppm as determined by McDonough and Sun (1995) is very high in comparison to the amount of sulphur that would be left after equilibrating with Fe-rich core material at the base of a deep magma ocean (20 to 100 ppm). So, assuming that mantle is chemically homogeneous and that the late veneer has the same S content as the CI chondrite, the veneer would account for 0.2 to 0.6% of the Earth's mass. This range fits the 0.34% mass of the Earth added as a late veneer estimated by Walker (2009) to be necessary to provide the abundances of highly siderophile elements (HSE) in the mantle, provided if the entire mantle has abundances similar to the estimates of the Earth's primitive upper mantle (PUM). McDonough and Sun (1995) argue for the presence of a late veneer from measuring the concentrations of the platinum-group elements in fertile peridotites and primitive basalts and komatiites. A relatively uniform Ni/Ir ratio in peridotites with little local variation argues for an effective re-homogenization of the silicate Earth after the addition of the late veneer.

During planetary accretion there would have been critical points of mass and temperature at which the segregation of material into cores, mantles and crusts began. For segregation to occur, the materials would have to be hot enough to be molten or have plastic behaviour. This heat has a number of potential sources. Christiansen (1995) lists some of the main sources of thermal energy for planetesimals. Radiogenic heat is derived from the spontaneous breakdown of unstable isotopes into daughter products, releasing energy as they do so. While there is no original ^{26}Al or ^{60}Fe left in the solar system (which decay to ^{26}Mg and ^{60}Ni, respectively), the longer-lived isotopes of U, Th and K are still a source of thermal energy within the planets. Accretionary heating occurs when early planetesimals collide and the kinetic energy of the collision is converted to thermal energy. A large enough impact could have completely melted the upper layers of a planetesimal; for example the collision thought to have produced the Earth's Moon. Once core formation had begun within these planetesimals, this process may have been a source of thermal energy for itself, as the gravitational

potential energy lost from each descending metallic “droplet” would have translated into a small thermal gain for the planetesimal. These are likely the main sources of thermal heating for planetesimals. Solar energy, while vital for the biological processes occurring on the surface of the Earth would not be sufficient for heating the planetary interior. There is also tidal energy, where the gravitational deformation of one planetary body by another larger one can generate heat. This would be insignificant in the case of the Earth and the Moon, but appears to be the source of energy for volcanic activity on Io, which is under constant gravitational strain from Jupiter. Peale *et al* (1979) describe the source of frictional heating as being caused by the eccentricity of Io’s orbit around Jupiter, which constantly exerting changing gravitational stress on its interior. Such tidal dissipation can go into circularising a moon’s orbit, but Io’s eccentric orbit is maintained by its 1:2:4 Laplace orbital resonance with Europa and Ganymede.

Baker *et al.* (2005) noted that the bodies that formed earlier in the solar system are differentiated as opposed to those that formed later, as the former had heat sourced from the decay of very short-lived isotopes that have long since all transformed into their daughter products. The two most common radionuclei at the time were ^{26}Al and ^{60}Fe. They found an age of approximately 4.5662 Ga based on Pb-Pb dating for basaltic angrite meteorites, which is only 1 Myr younger than the accepted minimum age of the solar system when the decay of ^{26}Al would still have been ongoing. The finding of small ^{26}Mg excesses in bulk angrite samples supports this further.

The different masses would result in different extents of segregation for the various planetary and asteroidal bodies. For example, according to Righter and Drake (1996), metal-silicate segregation on Vesta could have begun very early, with mantle-core equilibrium occurring at low pressures. Based on siderophile element abundances consistent with low-pressure liquid metal-liquid silicate equilibrium they estimated that Vesta’s core is 10% of its mass. Different scenarios need to be developed for Earth and Mars due to their differences in mass. It is likely that Mars underwent intermediate pressure metal-silicate

equilibration while Earth reached much higher internal pressures and temperatures.

It is already known from shock wave data that the density of the Earth's core is about 9-12% less than that of pure Fe-Ni alloy e.g. Mcqueen and Marsh (1966). To account for this discrepancy, there must be a light element component to the core of the Earth. The suggested light elements are S, C, H, O, K, N, He, Mg and Si. Any element with a lower atomic number than Fe could account for the reduced density of the core, but these particular elements have to fulfill three requirements as described by Wood (1993): a high cosmic abundance in the solar nebula, sufficient solubility in Fe-Ni alloys under outer core conditions and strong partitioning into liquid Fe metal during low pressure melting. Not all of these elements are soluble in Fe. The latter requirement comes from the observation that before the growing Earth reached even the size of Mars, impact heating and the decay of short-lived isotopes would cause from the surface downwards the melting of a metal-silicate Earth. In such a scenario, liquid Fe metal would begin to segregate from the silicate melt at pressure of 0 to 5 GPa, and not the 136 GPa of the current core-mantle boundary. The elements that are soluble in liquid Fe metal at 1atm are Si, C and S. Georg *et al.* (2007) observed that basaltic samples from Earth and Moon have similar Si isotopic compositions and that these differ slightly from carbonaceous chondrites. They concluded that the difference is consistent with dissolution of Si into the core and that the similarity between Earth and Moon indicates that Si dissolution occurred before the moon-forming impact. The accretionary model presented by Wade and Wood (2005) suggests a Si content if approximately 5-7%. However Si seems unlikely to account for the entire amounts of light element material present, given that for it to enter the core in sufficient quantities at low pressure, the oxygen fugacity would be have to be so reduced as to make Ti, an element also present in the Earth's mantle in chondritic quantities, enter the core. This leaves S and C as the most likely other elements for the light element component of the core. The chief questions for light elements is what is their total mass within the core, which light elements are involved and how much of each? Some constraints can be applied. For example, based on volatility and concentration in the solar nebula,

Dreibus and Palme (1996) estimated the amount of S in the core as 1.7 wt%. This was determined by the use of the abundance of Zn in the mantle. Zn has a similar volatility and concentration to S in the reduced conditions of the solar nebula, but is of lithophile character, so there is likely to be no Zn present in the core. By using the bulk Zn content of the mantle, estimated by Dreibus *et al.* (1979) from mantle xenoliths to be around 50 ppm, Dreibus and Palme calculated the bulk S content of the Earth by assuming a chondritic S/Zn ratio of 167, by weight for the bulk Earth. Their values of 0.56% for sulphur in the bulk Earth lead to a corresponding core content of 1.7%. The carbon content of the Earth cannot be constrained in the same way, but, if we assume that the C/S ratio of Earth is the same as in CI chondrites (a likely maximum value), we obtain a C content of the core of 1.1%. A plausible model would therefore entail 1.7% S, 1.1% C and 6% Si Shahar *et al.* (2009) in the core with the possibility of oxygen being added at the highest pressures of core segregation Rubie *et al.* (2004).

In order to mass balance the Earth's composition, another important area is the behaviour of siderophile elements, a group that preferentially dissolves into Fe-rich metallic liquid, over silicate melt. These elements have little affinity for oxygen and form metallic bonds with iron. The partition coefficients between metals (proxy for the Earth's core) and silicates (proxy for the Earth's mantle) have been extensively used as indicators of the extent to which a specific element enters the core. What are the partition coefficients of each element? A siderophile element that has gone mostly into the core is observed as depleted (relative to CI chondrite values) in the mantle. To date, there are many data in the literature on siderophile element partitioning between metal and silicate e.g. Righter (2011). It was pointed out some 50 years ago that the concentrations of siderophiles (notably Co, Ni) in the mantle are much higher than the values that low pressure partition coefficients suggest should be present. Ringwood (1966) called this the "excess siderophile problem". One possible interpretation of this observation is that core and mantle did not equilibrate with one another during metal segregation. Another possibility is that the conditions of equilibration were very different from those obtaining in low-pressure experiments and that pressure and or temperature has a large effect.

To explore on this topic deeper, the effects of a number of parameters that might have significant influences on the partition coefficients have been investigated. Pressure and temperature are important factors controlling partitioning of some of the elements. For instance, Li and Agee (1996) demonstrated that the current concentrations of Ni and Co in the mantle, which are inconsistent with low-pressure metal-silicate equilibration, would be consistent with metal-silicate equilibrium occurring at the base of the magma ocean at around 28 GPa. Kegler *et al.* (2008) reinvestigated Ni and Co partitioning over a wide range of temperatures and pressures (10^{-4} to 25 GPa and 1,300 to 2,300°C) and found that the mantle ratio for Co/Fe is obtained at 32 to 37 GPa while the Ni/Fe ratio requires equilibration at 45-50 GPa. They therefore concluded that high-pressure core segregation is the key to the Ni and Co contents of the mantle and that the hypothesis of a giant single-stage magma ocean forming most of the current concentrations of siderophile elements in the mantle is unlikely. Mann *et al.* (2009) looked for evidence of high-pressure core-mantle differentiation by examining the metal-silicate partitioning behaviour of a suite of lithophile and weakly siderophile elements (Ta, Nb, Cr, V, Si, Mn, Ga, In and Zn) under varying pressures and temperatures. They found that, to account for the mantle ratios of element pairs Ga-Mn and In-Zn, metal-silicate equilibration at pressures of at least 10-40 GPa are required.

Siebert *et al.* (2011) observed from metal-silicate partitioning experiments that increasing temperature results in increased siderophile character for V, Cr, Mn, Zn, Nb and Ta, while Ni, Co, Mo, Ge, and As become less siderophile. The changes in temperature didn't affect Ga, W and P. When they included the changes caused by increasing pressure and oxygen fugacity, they concluded the best model to fit the current concentrations of most of these elements in the mantle is continuous core formation at the base of a magma ocean. They argued that core segregation began at reduced conditions followed by progressive oxidation to the current mantle fO_2 conditions. This is also the conclusion reached in the earlier paper by Wade and Wood. (2005).

The use of siderophile element partitioning to infer increasing oxidation state during accretion leads to the question of whether it is reasonable to assume a

change from reduced to oxidised material accreting to the planets over time, or whether planetary mantles can self-oxidise (Wade and Wood 2005). Wanke (1981) uses the trends observed in the mantle of the Earth such as the depletion of V, Cr, and Mn by factors of 2-4 and the enrichment of all refractory lithophile elements and Mg by a mean factor of 1.3 relative to Si to propose an inhomogeneous accretion model. In it he claims the Earth began with highly reduced material without volatile elements, with some elements present in metallic form only, such as Fe, Co, Ni, Ga and W. Once two-thirds of the Earth had accreted, more oxidised material was added and then the last 20% of so was a mixture of highly oxidised material and moderately volatile elements in CI abundances. It was at this point that metallic Fe became unstable, which explains why the last 0.2% of the Earth's mass retained the highly siderophile elements in CI abundances ratios. O'Neill (1991) examined the siderophile concentrations patterns in the Earth's mantle and came to a conclusion similar to that of Wänke, but instead of a slower accretion of oxidised material later on, he suggests that this oxidised material was supplied in the form of the Impactor (later named Theia) that led to the formation of the Moon. If this was the case then the Impactor stands out as an exotic arrival to that area of the solar nebula where the Earth accreted, given its highly oxidised composition. Wade and Wood (2005) observed that the concentrations of refractory elements in the mantle are reasonable given initial conditions of 40GPa and 3,477°C. However, this is 700°C above the peridotite liquidus at 40GPa, the base of the magma ocean and thus physically unlikely. They found as long as the oxygen fugacity remained fixed to near-current mantle conditions, the peridotite liquidus doesn't match dynamic accretion models. It was suggested by them instead that once the stable conditions for magnesium perovskite were reached within the Earth, the perovskite layer acted as an oxygen pump that increased the redox state of the mantle. Mars is seen as not having undergone this process to the same extent given that perovskite would have only been stable close to the core-mantle boundary.

One distinct possibility is that the presence of light elements in the metal is not only the source of reduced density in planetary cores, but that it also influenced

the behaviour of the siderophile elements during accretion. The dissolution of Si in the metal affects the partitioning of a number of elements, reducing the siderophile character of Mo, W Ni and Co substantially, but having little effect on Cr, V and Nb (Tuff *et al.* 2011). Jana and Walker (1997) found that in the presence of carbon-saturated metal, P changes character completely and becomes lithophile (preferentially dissolves into silicate melt) instead of siderophile. Similar behaviour has been observed for Pb (Wood and Halliday, 2010). Thus, inferences about the conditions of accretion and core segregation based on element partitioning behaviour must depend on the concentrations of different light elements in the metal as well as the pressure-temperature path of accretion. As yet, however, there have been few studies performed to determine explicitly the effects of the light elements on partitioning of the most important siderophile elements.

Given the profound effects of Si and C on metal-silicate partitioning discussed above, it is clear that more experimental data on the effects of light elements on partitioning are required in order to build a reliable model of planetary accretion based on elemental abundances in the mantle. The aim of this project, therefore, is to determine experimentally at high pressures and temperatures the changes in siderophile behaviour of Co, Ni, Mo, W, Cu, Ag, Sb, Mn, Cd, Pb, Tl, V, Zn, Ge and Ga caused by the presence of the important low atomic number elements, sulphur and carbon.

Chapter 2. Experimental and analytical procedures

2.1. Experimental methods

All starting materials were based on a mix of 50-75% metal and 25-50% synthetic silicate, by weight. The silicate constituent was a composition close to the 1.5 GPa eutectic compositions in the system anorthite–diopside–forsterite ($An_{50}Di_{28}Fo_{22}$) Presnall *et al.* (1978) (Table 1)[1]. This composition was prepared by separately synthesizing Forsterite, Diopside and Anorthite from mixtures of reagent-grade oxides (SiO_2, Al_2O_3, MgO) and carbonates ($CaCO_3$). The oxides were fired overnight at 1100°C before weighing, while $CaCO_3$ was kept at 110°C before use. Intimate mixtures were prepared by grinding components together. Carbonate-free compositions were then pelletized and fired at 1300°C to react them. Carbonate-bearing starting materials were decarbonated at 800°C for ~24 hours, then pelletized and fired at 1300°C. Products were ground and re-pelletized and fired a further two times to ensure homogeneity. The three product silicates were mixed in the desired proportion and then doped with trace element mixes, which had been pre-prepared in large quantities from reagent-grade oxides. Most of the experiments were doped with the trace element mixture (TR) containing Mn, Ti, Cu, In, Tl, Pb, Ga, Ge, Ag, Zn, Cr, V, Co, Sb and Cd as oxides. Some experiments on very siderophile Ni, Co, Mo and W used higher abundances of these elements in order to obtain measureable concentrations of the trace element in the silicate. Iron oxide was added to the silicate mix as reagent grade "FeO" in order to adjust the oxygen fugacity of the experiment to the desired value. Pure Fe was usually used for the metal constituent, with the exception of the iron/iron sulphide experiments where a mixture of Fe and FeS was employed. Experiments were performed either in 6mm O.D., 2mm I.D. MgO capsules, 3mm O.D., 1.2 mm I.D. graphite capsules or 3mm/1mm silica glass capsules.

The use of different capsules served different purposes. The graphite capsules allowed compositions to be affected by saturation of the metal in carbon. The MgO capsules provided the reverse scenario with no carbon present. When it

[1] All the tables are located in the appendix

came to run experiments involving Co and Ni, it was found that these two trace elements are rapidly absorbed by the polycrystalline MgO, leaving virtually nothing in the sample compositions, even when run time was run as low as 5 minutes (Tuff *et al.* 2011). Replacement of the MgO capsule by silica glass eliminates this problem (Tuff *et al.* 2011) for Co and Ni.

Experiments were preformed at 1.5 GPa, using an end-loaded Boyd-England type piston-cylinder apparatus. All of the experiments used a half-inch $BaCO_3$-SiO_2 glass assembly with a 8mm O.D. 6mm I.D. graphite heater. The internal spacers consisted of 6mm diameter MgO that had been previously fired at 1,000°C to ensure dryness. Temperatures were measured and controlled at a nominal temperature of 1635°C using type C thermocouples ($W_{95}Re_5$-$W_{74}Re_{26}$), which were introduced into the centre of the cell, located just above the capsule and separated from it by a 1mm alumina disc. Temperatures are adjusted upwards by 15°C to take account of the distance between thermocouple tip and capsule. Experiment durations were 10-30 minutes. These experiment durations have previously been found to be sufficient to approach constant partitioning of trace elements for experiments in this size of capsule at this temperature and pressure (Tuff, Wood and Wade 2011; Wood and Halliday 2010).

All experiments were quenched by cutting power to the graphite heaters while maintaining water flow and run pressure, which was subsequently slowly released. The recovered products of the runs were sliced open longitudinally; mounted in acrylic resin, then ground using different grades of wet and dry paper. They were then polished using 1-micron diamond paste. During the experiment the charges invariably separated into metal and silicate liquids, which after quenching, produced blobs of metal surrounded by silicate phases which were either glass (graphite and silica capsules) or a mixture of glass and quench crystals (MgO capsules).

2.2. Major and minor element analyses

The experimental run-products were analysed using the JEOL JXA8600 electron microprobe at the Department of Archaeology at the University of Oxford. Wavelength dispersive (WDS) analyses were conducted using a 15 kV

accelerating voltage and 20 nA beam current with a defocused 10 micron spot to improve averaging of both silicate and metal phases. The defocused electron beam was used in order to reduce the risk of heterogeneities within the sample distorting the overall analysis. At least 25 repeat analyses were collected for the silicate and metal portions in each charge, with care being taken to avoid any possible secondary fluorescence arising from analyses that were too close to the edge of each phase (Wade and Wood, 2012). Counting times were as follows: 30 seconds peak and 15 seconds background for major elements (e.g. Si, Al, Ca, Mg, Fe) and 60-90 seconds peak with 30-45 seconds background for minor and trace elements. A range of synthetic and natural standards was used for calibration. Standards for metal analysis were metallic Mo, W, Ni, Co, Cu and hematite (Fe). Standards for silicate analysis were natural wollastonite (Ca, Si), synthetic periclase (Mg), natural albite (Al) and hematite (Fe). Natural almandine was used as a secondary standard for the silicate phases.

Trace-element concentrations of the co-existing silicate glasses and metals were determined on experimental products using Laser Ablation Inductively Coupled Mass Spectrometry (LA-ICPMS). Measurements were made using a Perkin Elmer Nexion quadrupole mass spectrometer coupled to a New Wave Research UP213 Nd:YAG laser at the University of Oxford. Beam diameters of 50 µm were used for both silicate and metal phases. The following masses were counted: ^{53}Cr, ^{55}Mn, ^{59}Co, ^{60}Ni, ^{65}Cu, ^{71}Ga, ^{74}Ge, ^{51}V, ^{47}Ti, ^{66}Zn, ^{107}Ag, ^{111}Cd, ^{115}In, ^{121}Sb, ^{205}Tl, ^{208}Pb, with yields calibrated on NIST 610 glass standard as the primary standard. NIST 612 glass and USGS glass standard BCR-2G were used as secondary standards to monitor the accuracy of the calibration. The NIST 610 calibration was routinely checked after every 10-15 unknowns and results corrected for calibration drift. Internal standards for the silicate and metal phases were principally the Si and Fe contents, respectively, which had been measured by electron microprobe. Because the Fe content of NIST 610 is only 460 ppm and backgrounds are high additional internal cross-checks are required for the metal analyses. Ni and Cu contents were therefore also measured by electron microprobe and re-measured using LA-ICPMS. The results of electron microprobe analyses, which are generally within 10 relative % of LA-ICPMS results for Ni are given in Tables 2-3

and Fig. 1. For Co, Mo and W, WDS values were used. The LA–ICPMS analyses (Tables 4-5) involved determining background counts for the first 20 seconds of each 60-second analysis and then collecting counts for each mass during the 40 sec period of ablation. Background was minimised by including a 60-second 'wash-out' between each collection. Raw counts were collected on the ICPMS in peak-hopping mode and displayed in time-resolved format. Data reduction used the GLITTER (www.es.mq.edu.au/gemoc/glitter) software package. This allowed each ablation to be monitored to identify heterogeneities such as small metal inclusions in the silicate and compositional variations with depth.

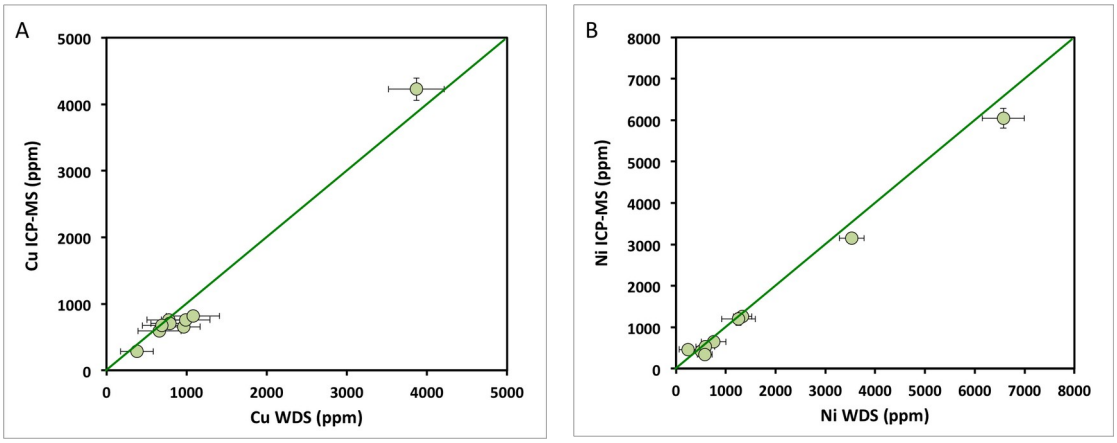

Fig. 1. A. ICP-MS vs. WDS data for Cu. B. ICP-MS vs. WDS data for Ni.

Chapter 3. Experimental results

Major and trace element compositions of metal and silicate phases from experimental products are presented in Tables 2-5. All of the trace elements added to the starting materials were above detection limits in both metal and silicates phases in all experiments and appear to be homogeneously distributed in both phases.

3.1. The exchange coefficients.

The partitioning of an element M, with valence *n*, between metal and silicate can be expressed as an exchange reaction involving Fe and FeO:

$$MO^{silicate}_{n/2} + n/2Fe^{metal} = M^{metal} + n/2\ FeO^{silicate} \quad (1),$$

For which the equilibrium constant *K* can be written as

(2),

With *a*, *X* and γ being the component's activities, mole fractions and activity coefficients, respectively. If we define an exchange coefficient K_D for any element M:

$$K_D^M = \frac{[X_M^{metal}][X_{FeO}^{silicate}]^{n/2}}{[X_{MOn/2}^{silicate}][X_{Fe}^{metal}]^{n/2}} \quad (3)$$

Then Equation 2 can be rearranged to give:

$$LogK_D^M(P,T) = -\log K - \log\left[\frac{[\gamma_M^{metal}]}{[\gamma_{Fe}^{metal}]^{n/2}}\right] - \log\left[\frac{[\gamma_{FeO}^{silicate}]^{n/2}}{[\gamma_{MOn/2}^{silicate}]}\right] \quad (4)$$

If the valence *n* is correctly determined, K_D should be independent of fO_2. It does, however, depend on the activity coefficients of metal and oxide components in metallic and silicate phases respectively. The aim of the experimental program

was to work under conditions where the silicate melt composition remains essentially constant while the metal composition changes substantially in the concentration of either S or C. Thus, the ratio of oxide activity coefficients in the silicate (last term on the right hand side of equation (4) is essentially fixed, while the ratio of activity coefficients in the metal (penultimate term) is responding to variations in metal composition. As will be shown below, the response of K_D to metal composition is large for some elements and I need to model for activity-composition relationships for this phase in order to understand and interpret the S and C effects on partitioning.

Wade and Wood (2005) introduced the use of the ε-model for metals to the geological literature. When corrected to obey the Gibbs-Duhem equation (Ma, 2001) model gives the following expressions for activity coefficients of Fe and of the dilute solute components I (Ma, 2001):

$$\ln\gamma_{Fe}^{met} = \sum_{i=2}^{N}\varepsilon_i^j(x_i + \ln(1-x_i)) - \sum_{j=2}^{N-1}\sum_{k=j+1}^{N}\varepsilon_j^k x_j x_k\left(1+\frac{\ln(1-x_j)}{x_j}+\frac{\ln(1-x_k)}{x_k}\right)$$
$$+\sum_{\substack{i=2\\k\neq i}}^{N}\sum_{k=2}^{N}\varepsilon_i^k x_i x_k\left(1+\frac{\ln(1-x_k)}{x_k}-\frac{1}{1-x_i}\right)+\frac{1}{2}\sum_{j=2}^{N-1}\sum_{k=j+1}^{N}\varepsilon_j^k x_j^2 x_k^2\left(\frac{1}{(1-x_j)}+\frac{1}{(1-x_k)}-1\right)$$
$$-\sum_{\substack{i=2\\k\neq i}}^{N}\sum_{k=2}^{N}\varepsilon_i^k x_i^2 x_k^2\left(\frac{1}{1-x_i}+\frac{1}{1-x_k}+\frac{x_i}{2(1-x_i)^2}-1\right) \qquad (5)$$

$$\ln\gamma_i^{met} = \ln\gamma_{Fe}^{met} + \ln\gamma_i^{o} - \varepsilon_i^i\ln(1-x_i)$$
$$-\sum_{\substack{k=2\\k\neq i}}^{N}\varepsilon_i^k x_k\left(1+\frac{\ln(1-x_k)}{x_k}-\frac{1}{1-x_i}\right)$$
$$+\sum_{\substack{k=2\\k\neq i}}^{N}\varepsilon_i^k x_k^2 x_i\left(\frac{1}{1-x_i}+\frac{1}{1-x_k}+\frac{x_i}{2(1-x_i)^2}-1\right) \qquad (6)$$

In equations (5) and (6) x_i refers to the mole fraction of i in the metal γ_i^{met} is the activity coefficient of i, γ_i^{o} is the activity coefficient of i infinitely dilute in liquid Fe

and ε_i^j is the interaction parameter between elements i and j. Deviations from Henry's Law are accounted for by the ε_i^j terms. The principal reason for using this approach is that many interaction parameters have been experimentally measured and are presented in the form of ε_i^j values (Steelmaking, 1988). In the discussion, which follows, ε_i^j values have been extrapolated from 1873K to the experimental temperatures of 1923K (for the Ni, Co, Mo and W) and of 1823 (for Cu, Cr, Ge, Mn, Pb and V), using the relationship from the Steelmaking Data Sourcebook:

$$\varepsilon_i^j(T) = \frac{1873}{T}\varepsilon_i^j(1873)$$

Activity coefficients for Fe in the metal, γ_{Fe}^{met} were obtained from the database and online calculator hosted on the Oxford website http://www.earth.ox.ac.uk/~expet/metalact/. The experimental data presented here were then used to estimate the ε_i^j values for the solute elements of interest.

3.2. Partitioning of Ni and Co

Figures 2a and 2b compare the K_D of Ni and Co versus the concentration of sulphur in metal, as weight %. For both Ni and Co there is a decrease in K_D value as the % of sulphur increases. For Ni there is a decrease from values of about 200 at pure Fe to 50 at pure FeS. Co decreases from 30 at pure Fe to 5.5 at FeS. It is also noted that the K_D values for Ni at the highest concentrations of sulphur are an order of magnitude greater than the K_D values for Co.

Figures 2c and 2d show the K_D of Ni and Co versus the weight % of carbon in the metal. The solubility of carbon in metal at 1.5 GPa and 1635°C is about 5.5 wt% (data from the metal activity calculator). The rest of the experiments were

performed in MgO or SiO_2 capsules and therefore contain 0% C in the metal. The effects of C on the Ni and Co partitioning are evident. K_D for Ni declines from an average Kd value of 200 at 0 wt% C to approximately 80 at 5.5 wt% carbon. Kd for Co decreases from 30 to an average value of 15.

Treatment of the effects of S and C on the partition coefficients for Ni and Co can be performed in terms of the ε-model for the metal by assuming that the activity coefficient ratio for the oxide components in the silicate (last term on right hand side of equation 4) is constant as the S and C contents of the metal are varied. Then, since log K is a constant at fixed temperature and pressure we have, using natural logarithms:

$$\ln K_D = Const + \frac{n}{2}\ln \gamma_{Fe}^{met} - \ln \gamma_i^{met} \quad (7)$$

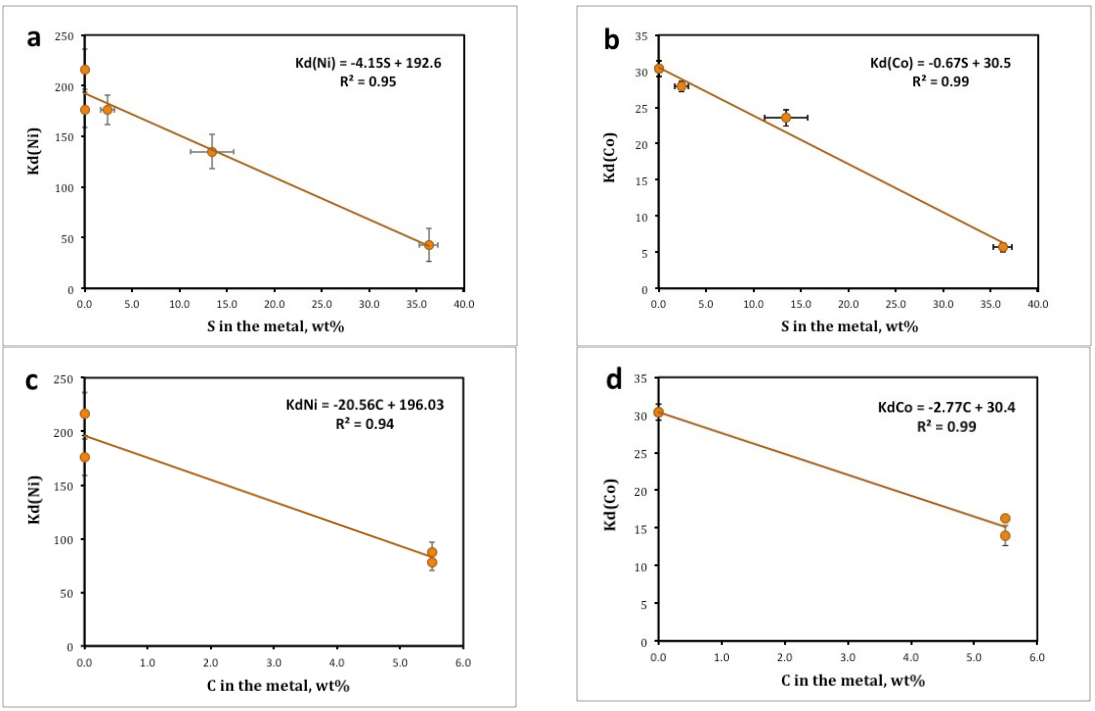

Figure 2. (a). Kd values for Ni versus wt% S. (b). Kd values for Co versus wt% S. (c) Kd values for Ni versus wt% C. (d). Kd values for Co versus wt% C.

Noting that Ni, Co and Fe all have the same +2 oxidation state in the silicate at metal saturation and assuming that Ni and Co are infinitely dilute in the metal, we substitute the activity coefficient expressions (5) and (6) into equation (7) with the following result:

$$\ln K_D = Const - \ln \gamma_i^0 + \varepsilon_i^k \ln(1 - x_k) \quad (8)$$

Since γ_i^0 is also a constant at fixed pressure and temperature, a plot of $\ln K_D$ versus $\ln(1-X_S)$ or $\ln(1-X_C)$ yields a slope which gives the epsilon parameters ε_i^S or ε_i^C (Fig.3).

I fitted equation (8) to my data on an element by element basis using the linear regression model of the SPSS statistical package. This generated the fitted lines shown in figures with epsilon parameter and fit parameters given in Table 6.

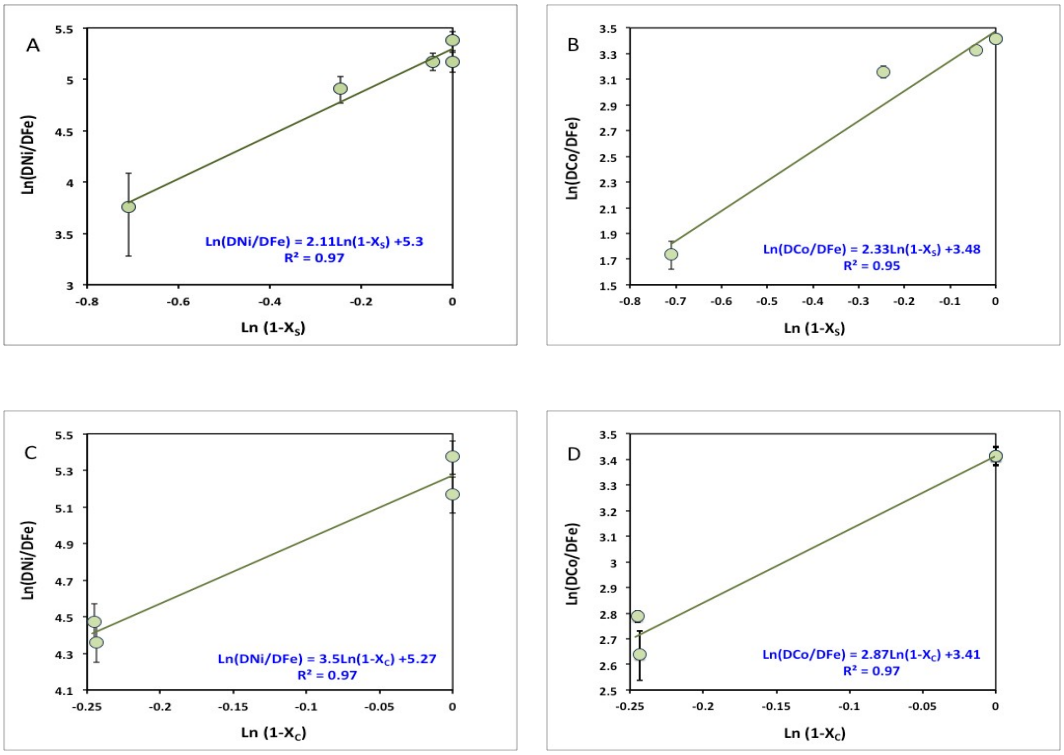

Figure 3. Effect of S and C on Ni and Co partitioning between metal and silicate liquids. The slope of the regression line yields the interaction parameter epsilon. (a) ε_{Ni}^S, (b) ε_{Co}^S, (c) ε_{Ni}^C, (d) ε_{Co}^C.

As can be seen on Fig. 3, partitioning of Ni and Co between silicate and metal is dependent on the sulphur content of the metal and decreases with the increasing amount of S. ε_{Ni}^S is 2.11 (±0.19) and ε_{Co}^S is 2.33 (±0.27). In comparison with the

tabulated values of -0.05 and of 0.60 for the ε_{Ni}^{S} and ε_{Co}^{S}, respectively (Steelmaking, 1988), both Ni and Co are much more dependent on the S-content of the Fe.

Values obtained for ε_{Ni}^{C} and ε_{Co}^{C} are 3.50 (±0.48) and 2.87 (±0.31), respectively. This is in a good agreement with the Steelmaking Data Sourcebook, which reports ε_{Ni}^{C} of 2.5 and ε_{Co}^{C} of 1.87.

Overall, partitioning of both Ni and Co is equally dependent on S and C content of the metal, and in all cases, the higher the proportion of S or C, the lower the partition coefficient for Ni and Co between metal and silicate.

The effect of $\ln \gamma_{Fe}^{met}$ cancels out only for divalent cations, for which n=2, while for the elements with different oxidation states, we need to apply a correction. For 1+ cations:

$$\ln K_D = Const - \frac{1}{2}\ln \gamma_{Fe}^{met} + \varepsilon_i^S(\ln(1 - x_S))$$

For 3+ cations:

$$\ln K_D = Const + \frac{1}{2}\ln \gamma_{Fe}^{met} + \varepsilon_i^S(\ln(1 - x_S))$$

For 4+

$$\ln K_D = Const + \ln \gamma_{Fe}^{met} + \varepsilon_i^S(\ln(1 - x_S))$$

For 6+

$$\ln K_D = Const + 2\ln \gamma_{Fe}^{met} + \varepsilon_i^S(\ln(1 - x_S))$$

All the elements on Figs. 4-6 are plotted according to their oxidation states considering the effect of $\ln \gamma_{Fe}^{met}$.

3.3. Partitioning of Mo and W

Figures 4a and 4b compare the K_D of Mo and W versus the concentration of sulphur in metal, as weight %. For both Mo and W there is a decrease in K_D value as the % of sulphur increases. For Mo there is a steep decrease from values of about 13 at 0 wt% Ni to 0.75 at around 36 wt% S. W also steeply decreases from 0.01 at 0 wt% S to $9x10^{-6}$ at 36 wt% S. It is also noted that the K_D values for Mo at the highest concentrations of sulphur are three orders of magnitude greater than the K_D values for W.

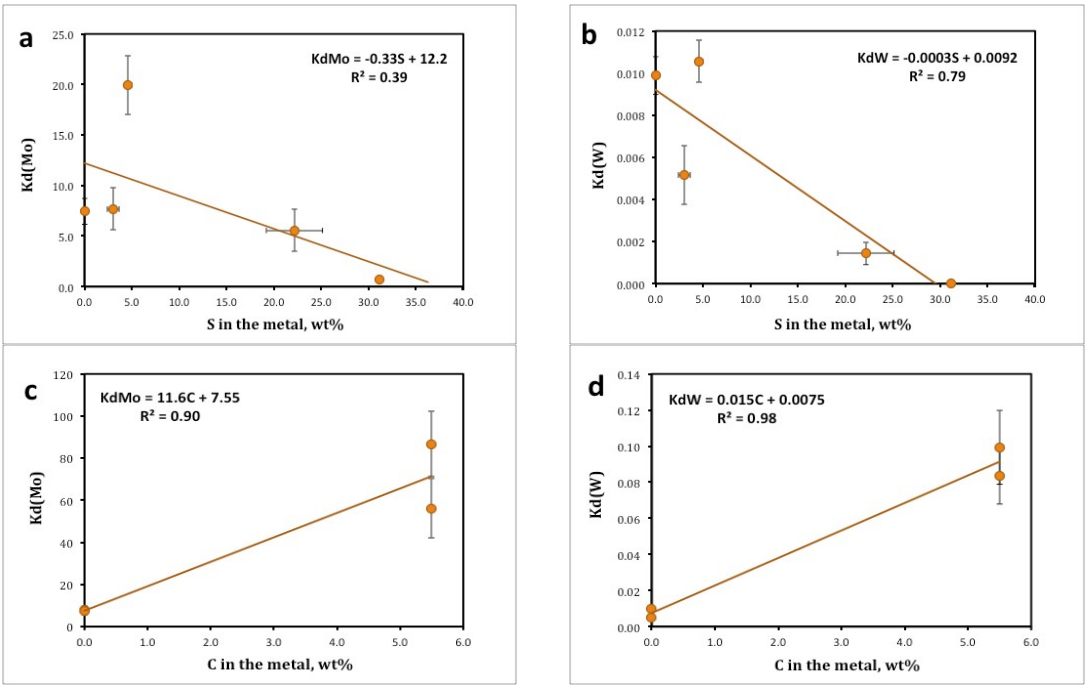

Figure 4. (a). Kd value of Mo versus wt% S. (b). Kd value of W versus wt% S. (c). Kd value of Mo versus wt% C. (d). Kd value of W versus wt% C.

Figures 4c and 4d show the K_D of Mo and W versus the weight % of carbon in the metal. The solubility of carbon in metal at 1.5 GPa and 1635°C is about 5.5 wt% (data from the metal activity calculator). The rest of the experiments were performed in MgO or SiO_2 capsules and therefore contain 0% C in the metal. The effects of C on the Mo and W partitioning are evident. K_D for Mo increases from an average Kd value of 10 at 0 wt% C to values of 50 and 90 at 5.5 wt% carbon. Kd for W increases from 0.01 to values of 0.08 and 0.1. The presence for two

differing values at 5.5% C is due to the presence of 5% FeO having been added to the silicate component of A245, compared to A244, which had no excess Fe as FeO added. For Mo, there is an increase in $\ln K_D$ values from 4.02 to 4.46 in the presence of FeO, while for W there is a slight decrease from $\ln K_D$ values from -0.26 to -0.46.

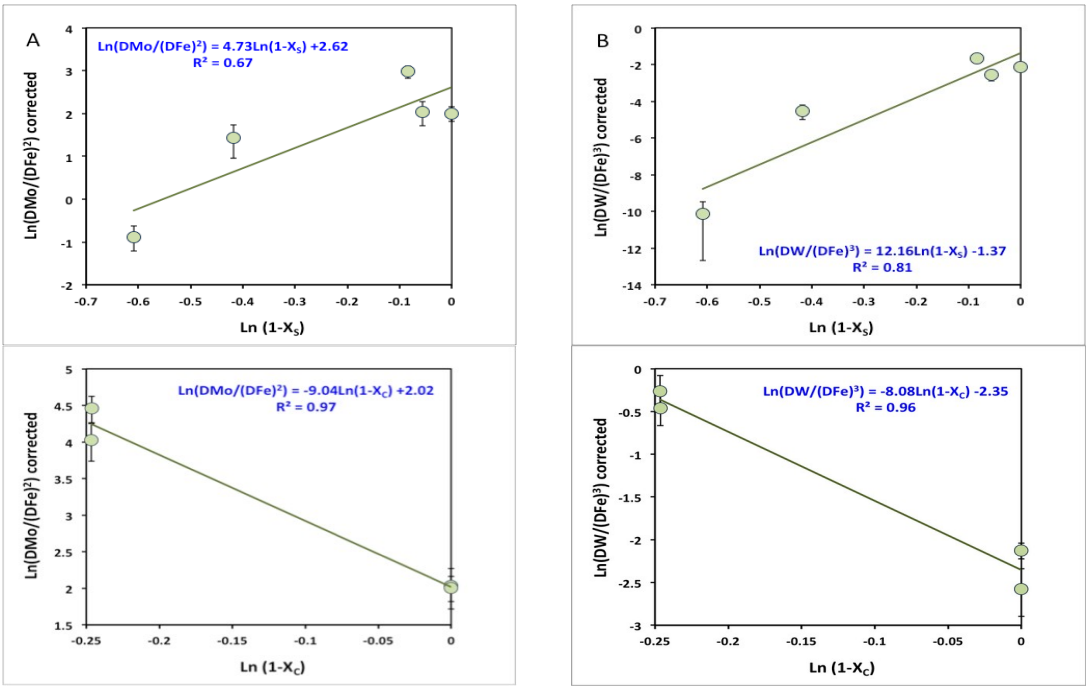

Figure 5. Effect of S and C on Mo and W partitioning between metal and silicate liquids. The slope of the regression line yields the interaction parameter epsilon. (a) ε^S_{Mo}, (b) ε^S_W, (c) ε^C_{Mo}, (d) ε^C_W.

The epsilon values for Mo and W (Fig. 5) are much higher than for Ni and Co, which suggests that the partitioning of these elements is much more dependent on the amount of S and C in metal.

In this study I obtained the values of 4.73 (±1.55) for ε^S_{Mo} and 12.16 (±2.87) for ε^S_W. This dramatic difference between Mo and W behavior is fairly predictable, because even though both metals are highly siderophile, molybdenum is much more chalcophile than tungsten and forms its own sulphide MoS_2 in nature. Even though the absolute values differ, the reported in literature values for the epsilon interaction parameter are an order of magnitude higher for W. The tabulated

values from the Steelmaking Data Sourcebook are 0.36 and 6.45 for ε_{Mo}^{S} and ε_{W}^{S}, respectively.

Both of metals show similar strong effect of C on their partitioning (Fig. 5). ε_{Mo}^{C} and ε_{W}^{C} measured by me are -9.04 (±0.88) and -8.08 (±1.0), respectively. These values agree well with those reported by the Steelmaking Data Sourcebook (-6.32 for ε_{Mo}^{C} and -7.01 for ε_{W}^{C}).

3.4. Partitioning of Cu, Mn, Ag, Sb, Cd, In, Tl, Pb, Ga, Ge, Cr, V and Zn

Apart from analysing how C and S effect the partitioning of Mo, W, Ni and Co between metal and silicate, I have obtained the data for a set of other chalcophile and moderately chalcophile metals. These data can be particularly useful for metallurgy and steelmaking as well as for modeling the Earth accretion and potential segregation of sulphide matte at the early stages of Earth formation.

The data has been obtained for a number of highly chalcophile (Cu, Ag, Cd, Pb, Tl, In, Sb) as well as for moderately chalcophile (Mn, Ga, Ge, Cr, V, Zn) metals. Apart from indium, which, possibly, has been lost to the MgO capsule in the runs with low sulphur content (up to 6 wt% S), all of the elements show consistent dependency and R^2 no lower than 0.66. As expected, the epsilon values for highly chalcophile elements (apart from In and Sb) are negative, which means that this metal is more likely to partition into the metal with the increasing S-content.

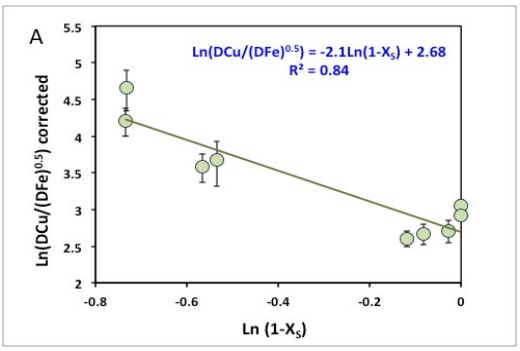

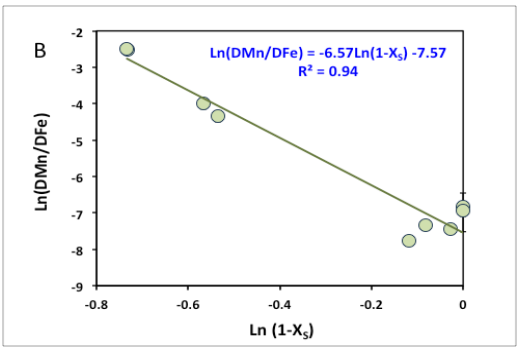

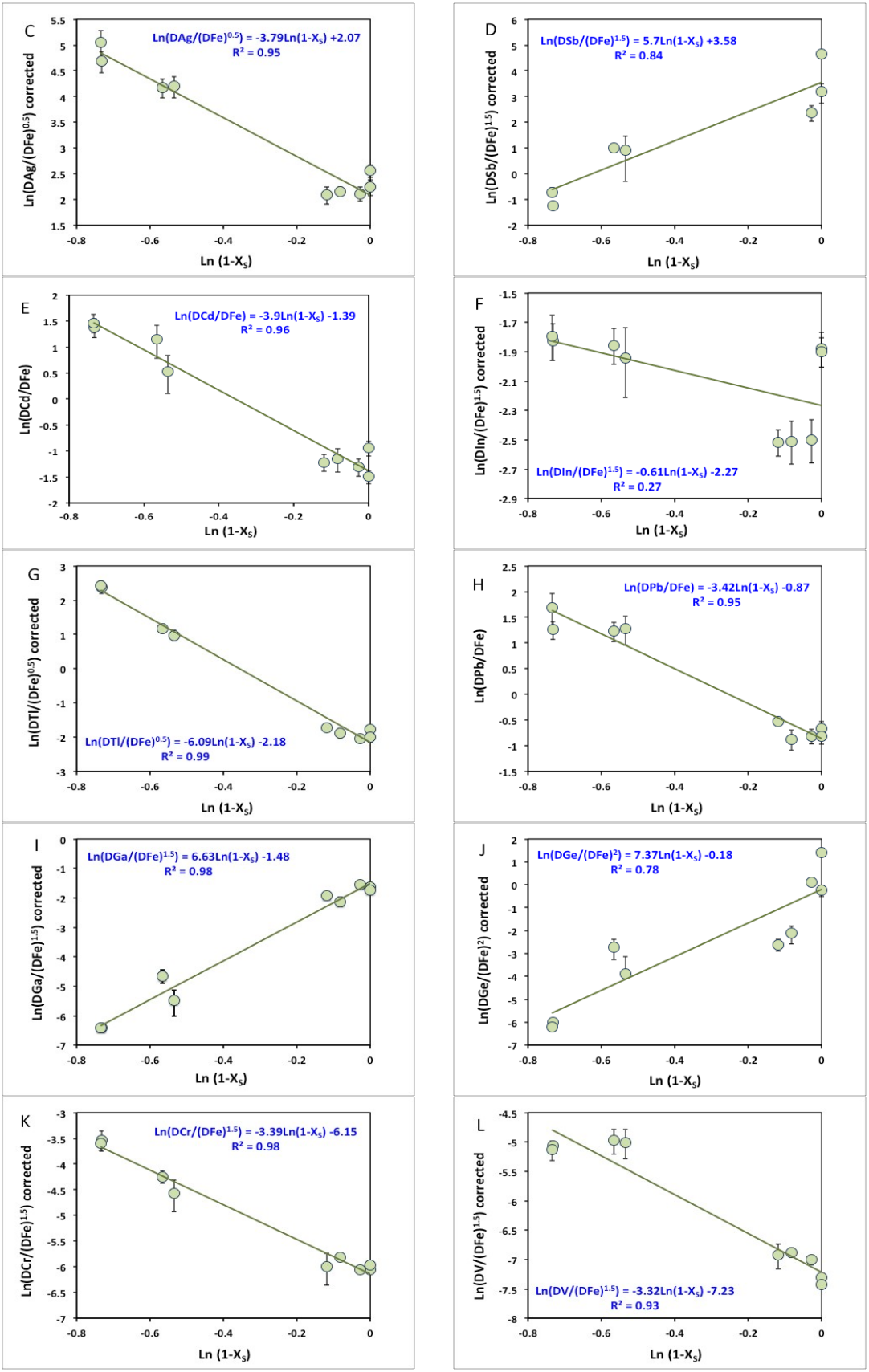
C
Ln(DAg/(DFe)^0.5) = -3.79Ln(1-Xs) +2.07
R² = 0.95
Ln(DAg/(DFe)^0.5) corrected
Ln (1-Xs)
D
Ln(DSb/(DFe)^1.5) = 5.7Ln(1-Xs) +3.58
R² = 0.84
Ln(DSb/(DFe)^1.5) corrected
Ln (1-Xs)
E
Ln(DCd/DFe) = -3.9Ln(1-Xs) -1.39
R² = 0.96
Ln(DCd/DFe)
Ln (1-Xs)
F
Ln(DIn/(DFe)^1.5) = -0.61Ln(1-Xs) -2.27
R² = 0.27
Ln(DIn/(DFe)^1.5) corrected
Ln (1-Xs)
G
Ln(DTl/(DFe)^0.5) = -6.09Ln(1-Xs) -2.18
R² = 0.99
Ln(DTl/(DFe)^0.5) corrected
Ln (1-Xs)
H
Ln(DPb/DFe) = -3.42Ln(1-Xs) -0.87
R² = 0.95
Ln(DPb/DFe)
Ln (1-Xs)
I
Ln(DGa/(DFe)^1.5) = 6.63Ln(1-Xs) -1.48
R² = 0.98
Ln(DGa/(DFe)^1.5) corrected
Ln (1-Xs)
J
Ln(DGe/(DFe)^2) = 7.37Ln(1-Xs) -0.18
R² = 0.78
Ln(DGe/(DFe)^2) corrected
Ln (1-Xs)
K
Ln(DCr/(DFe)^1.5) = -3.39Ln(1-Xs) -6.15
R² = 0.98
Ln(DCr/(DFe)^1.5) corrected
Ln (1-Xs)
L
Ln(DV/(DFe)^1.5) = -3.32Ln(1-Xs) -7.23
R² = 0.93
Ln(DV/(DFe)^1.5) corrected
Ln (1-Xs)

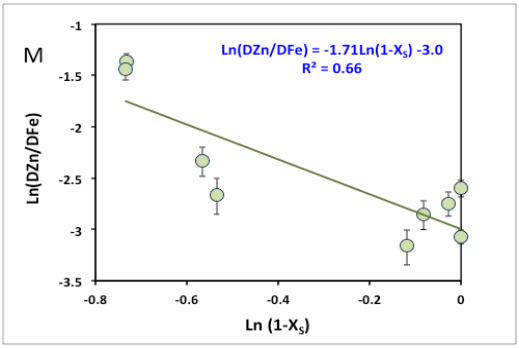

Figure 6. Effect of S on chalcophile and moderately chalcophile element partitioning between metal and silicate liquids. The slope of the regression line yields the interaction parameter epsilon. (a) ε_{Cu}^{S}, (b) ε_{Mn}^{S}, (c) ε_{Ag}^{S}, (d) ε_{Sb}^{S}, (e) ε_{Cd}^{S}, (f) ε_{In}^{S}, (g) ε_{Tl}^{S}, (h) ε_{Pb}^{S}, (i) ε_{Ga}^{S}, (j) ε_{Ge}^{S}, (k) ε_{Cr}^{S}, (l) ε_{V}^{S}, (m) ε_{Zn}^{S}.

Partition coefficients for Zn, Cr and V are also higher at the elevated S-contents. On the other hand, Ga, Ge and Sb show quite a strong preference to the metal. I could find the data only for a few elements in literature, and it generally compares well with the results of this study.

ε_{Cu}^{S} value listed in the Steelmaking Data Sourcebook is -2.35 (while I get -2.12±0.33), ε_{Mn}^{S} is reported -5.92 (my value -6.57±0.59), ε_{V}^{S} is -3.94 (my value -3.32±0.33), $\varepsilon_{Ge}^{S}$is 3.86 with my value slightly higher 7.37±1.35. Cr and Pb are reported much more chalcophile than I measure, with ε_{Cr}^{S} and ε_{Pb}^{S} -21.47 and -44.33 respectively (with my values of -3.39±0.17 for ε_{Cr}^{S} and -3.45±0.27 for ε_{Pb}^{S}).

Given that most of the interaction parameters, listen in the Steelmaking Data Sourcebook have been obtained for purposes of quantifying the effect of this or that metal on the sulphur (for instance, as ε_{S}^{Cr} , as opposed to ε_{Cr}^{S}), the values I am getting in this study, are more robust.

Chapter 4. Discussion and Conclusions

It has been known for some years (Li and Agee 1996; Thibault and Walter 1995) that partitioning of Ni and Co between metal and silicate depend strongly on pressure and that the observed Ni and Co contents of the silicate Earth imply pressures of metal-silicate equilibrium of greater than 25 GPa. When metal-silicate partitioning for other refractory elements, notably weakly siderophile V, Cr and Nb are considered together with partitioning for Ni, Co and W (Wade and Wood 2005; Wood *et al.* 2008) much better constraints on core formation emerge. In order to satisfy the estimated core-mantle partitioning of V, Ni and Co derived from their abundances in the silicate Earth, pressures of core formation would be close to 42 GPa with temperatures about 4500K, 1300° above the liquidus temperature of the mantle. The result, would be a core containing about 4 times as much Nb and Si as are plausible based on the abundances of these elements in silicate Earth (Allegre *et al.* 1995; Tuff *et al.* 2011). In order to match the estimated core-mantle partitioning, Wade and Wood (2005) constructed a model consistent with the physical concept of a deep magma ocean. In this model, accreting material is added to the upper mantle and the added metal is equilibrated with the mantle before accumulating in a layer at intermediate depth. The latter corresponds to the depth of the magma ocean and the point at which the underlying mantle becomes solid. Gravitational instabilities of the metal layer lead to periodic generation of large diapirs (Stevenson, 1981), which sink rapidly to the core without further equilibration. The implication is that the final metal-silicate equilibration temperature is close to the liquidus of the mantle silicate at some intermediate depth. In this case it is possible to grow the Earth with temperatures fixed on the silicate liquidus and match the Ni, Co, W, V, Cr and Nb contents of the silicate Earth. From Ni and Co partitioning, the magma ocean is calculated to maintain a thickness approximately 35% of the depth to the core-mantle boundary in the growing Earth. In order to satisfy the V, Cr and Nb contents of the mantle, however, it is necessary that much of the Earth accreted under conditions much more reducing than those corresponding to the current oxidized mantle Fe content of 6.26%. If there is no change in oxidation

state, V appears not to be siderophile enough. At low pressures and oxygen fugacities corresponding to the current Fe content of the mantle, Cr, V, Si and Nb are essentially lithophile while Ni, Co Mo and W are strongly siderophile. As oxygen fugacity is reduced, Cr, V and Nb eventually become somewhat siderophile, Si remains lithophile and Ni, Co and W remain strongly siderophile. Increasing pressure and temperature as the planet grows leads to increasingly siderophile character of Cr, V, Nb and Si while Ni, Co W and Mo become less siderophile (Thibault and Walter 1995; Wade, *et al*. 2012). Matching of the overall partition coefficients with values estimated from the composition of the mantle therefore requires a balance between pressure/temperature conditions, which increase with increasing planet size and the oxygen fugacity of core segregation. In practice Wood *et al*. (2008) found that V, Cr and Nb core-mantle partitioning is reproduced if the oxidized Fe content of the mantle increased from ~1% to the current value of 6.26% as the Earth grew. Their model also reproduces the calculated core-mantle partitioning of Ni, Co and W and yields a Si content of the core of approximately 7%, in good agreement with cosmochemical estimates (Allègre *et al.* 1995) and with inferences based on the difference between the Si isotopic composition of silicate Earth and that of carbonaceous chondrites (Shahar *et al.* 2009)

In the current study, I have investigated the effects of C and S on partitioning of the important refractory elements Ni, Co, W and Mo into Fe-rich metal during accretion. I have also determined the effects of S on the partitioning of a suite of refractory and volatile trace elements. As discussed in the introduction it is implausible that C and S comprise the sole components of the light element budget of the core and there is both cosmochemical and isotopic evidence in favour of a significant amount of Si joining them. The increasing oxidation state of the Earth during accretion proposed by Wade and Wood (2005) is consistent with a significant Si content of the segregating core. The latter feedback into the partitioning of, in particular, Ni, Co, Mo, W, the principal elements that constrain the pressure of equilibration. Since these elements all become less siderophile with increasing Si content of the metal (Figs. 4 and 5) the net effect should be to lower the pressure of equilibration given by their core-mantle partitioning. In addition, it has recently been shown that oxygen is to some extent soluble in

liquid Fe at high pressures and temperatures (Asahara *et al.* 2007; Ozawa *et al.* 2008). This element is known to interact strongly with V and Nb in the metal, making them much more siderophile (Corgne *et al.* 2009), so that the dissolution of oxygen should not be ignored when constructing core segregation scenarios.

In order to test the influence of light elements on partitioning into the core it is necessary to develop an internally consistent model in which pressure, temperature and oxygen fugacity (expressed as $D_{Fe} = \frac{[Fe]_{metal}}{[Fe]_{silicate}}$ where Fe in the silicate is oxidized) are factored into the partitioning of the light elements as well as the siderophile elements of interest. In this case both C and S are essentially completely siderophile, so their concentrations in the silicate can be ignored. However, Si and O are only weakly siderophile, so it is necessary to take account of the pressure and temperature dependences of their partitioning into the metal.

4.1 A continuous accretion model taking account of Si and O as "light elements"

In order to determine the impact of my new measured interaction parameters for S and C on the continuous growth and oxidation model of Wade and Wood, I incorporated the Si partition coefficient equation of Tuff *et al* (2011) and added the oxygen solubility model of Ozawa *et al.* (2008). The Earth was then grown in 1% increments, keeping the temperature of equilibration on the silicate liquidus (Tronnes and Frost, 2002; Zerr *et al.* 1998; Zhang and Herzberg 1994) ignoring the possible presence of C and S but accounting for pressure increase during accretion by taking equilibration pressure as a fixed fraction of the increasing pressure at the core-mantle boundary. At each step explicit account was taken of O and Si on metal-silicate partitioning of the elements of interest. Partitioning of the pressure-sensitive elements Ni, Co Mo and W constrains the pressure to be maintained at ~28% of the pressure at the core-mantle boundary which leads to a maximum pressure of ~36 GPa as shown in Figure 7. The overall result is relatively insensitive to the oxygen fugacity path taken during accretion because,

as shown in Figure 6, Ni, Co, Mo and W are only significantly retained in the mantle during the latest high pressure, high fO_2 stages of core segregation.

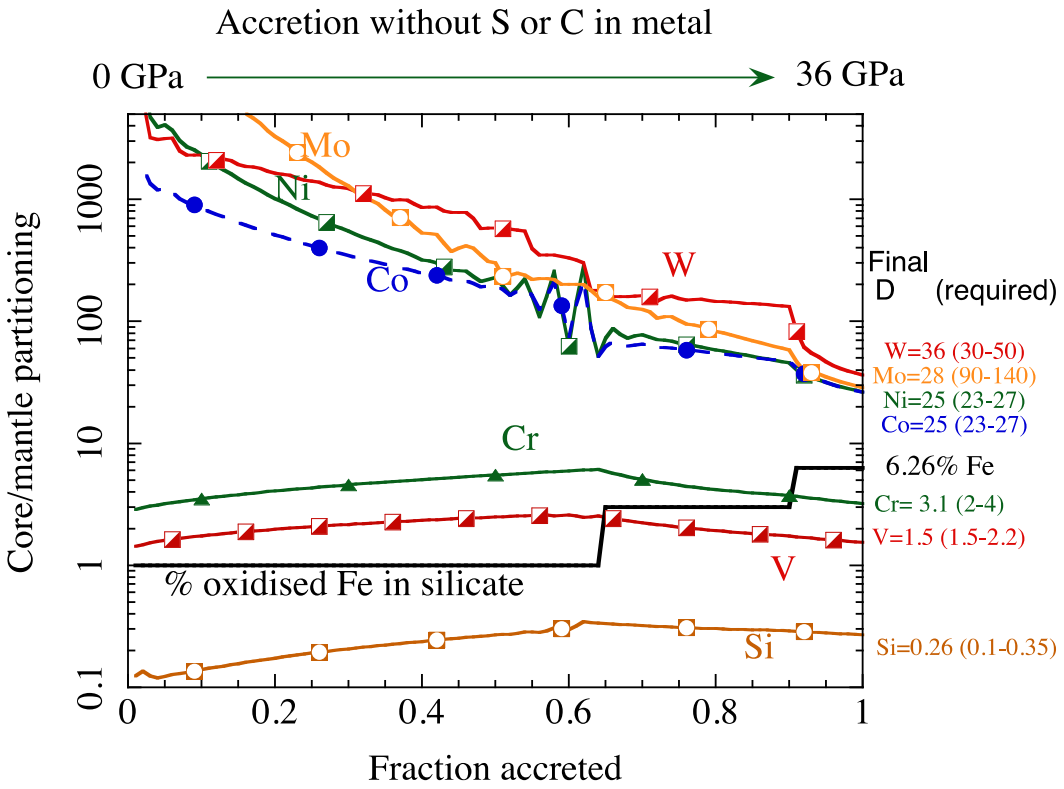

Fig. 7. Continuous accretion model, which reproduces the estimated core–mantle partitioning behaviour of Table 7. Note that oxygen fugacity, as represented by the oxidised Fe content of the mantle must, during most of accretion, be substantially lower than implied by the current oxidised Fe content of the mantle. Interactions of siderophile elements with Si and O were explicitly considered during accretion and the resulting model implies ~4.3 wt.% Si and 0.15% O in the core. Metal–silicate partitioning data, adjusted within uncertainty to improve fit, were taken from Wade and Wood (2005) for Ni, Co, Wood *et al.* (2008) for V, Cr, Nb, Wade *et al.* 2012 for Mo and Cottrell *et al.* (2009) for W.

The main problem with the result is that, although Ni, Co and W partitioning between core and mantle can be well matched with this type of model, it is impossible to obtain the correct Mo/W ratio of the silicate Earth unless the pressure is substantially lower than the final pressure shown in the Figure 6. On the other hand, observed Ni and Co partitioning between mantle and core require pressures of >30 GPa in this study and in all other studies which have

addressed conditions of Earth accretion. One possibility is that addition of S and/ or C to the core will change Mo: W relationships. This will be discussed in more detail below. Before considering addition of these light elements, it is appropriate to outline the additional properties of this "baseline" model.

As in previously published work with similar models (Wade and Wood, 2005), the only way to match the concentrations of V and Cr in the silicate Earth with the partition coefficients of Table 7 was to allow the Earth to oxidise as accretion progressed, as shown in Figure 7. The pressures and temperatures consistent with partitioning of Ni, Co and W between core and mantle in the presence of Si mean that the constraints on reducing conditions during accretion to explain V and Cr partitioning are stringent, as shown in Figure 7. Assuming that the last 10% of partitioning was at the current oxidised Fe content of the mantle (6.26%) most of accretion must have taken place under substantially more reducing conditions and this has been accounted for by allowing the mantle to oxidise in 2 steps from 1.0% Fe to the final value of 6.26%. The resultant Si and O contents of the mantle are 5.4 weight % and 0.15% respectively. The value of 5.4 wt% Si in the core is in agreement with an estimate based on experimental measurements of Si isotope partitioning between metal and silicate (Shahar *et al.* 2009). These authors concluded that the observed δ^{30}Si of silicate Earth implies that the core contains 2-6 weight % Si.

4.2 Continuous accretion with S, C, Si and O as "light elements"

Given the presence of S (~1.7%) and C (up to 1.1%) in the core these elements were added to the accretionary model described above, initially by assuming that each increment of added metal contains 1.7% S and 1.1% C i.e. that accretion is homogeneous. Figure 8 shows the results of the same kind of accretionary model, in which Earth is accreted in 1% intervals and the silicate is equilibrated with each increment of segregating metal, with the latter containing 1.7% S and 1.1% C. In this case the epsilon-parameters for the metal derived in this study were used, together with additional parameters from the steelmaking handbook where necessary. As can be seen the effects on most elements are small, but Mo now partitions more strongly into the metal than W. The effect is not, however,

sufficient to bring the partitioning of Mo between mantle and core into agreement with the expected partitioning of Table 7.

The assumption of homogeneous accretion has been called into question in a number of recent studies (Albarède 2009; Schönbächler *et al.* 2010) with it considered more likely that volatile elements such as S and C were delivered to Earth predominantly during the later stages of accretion.

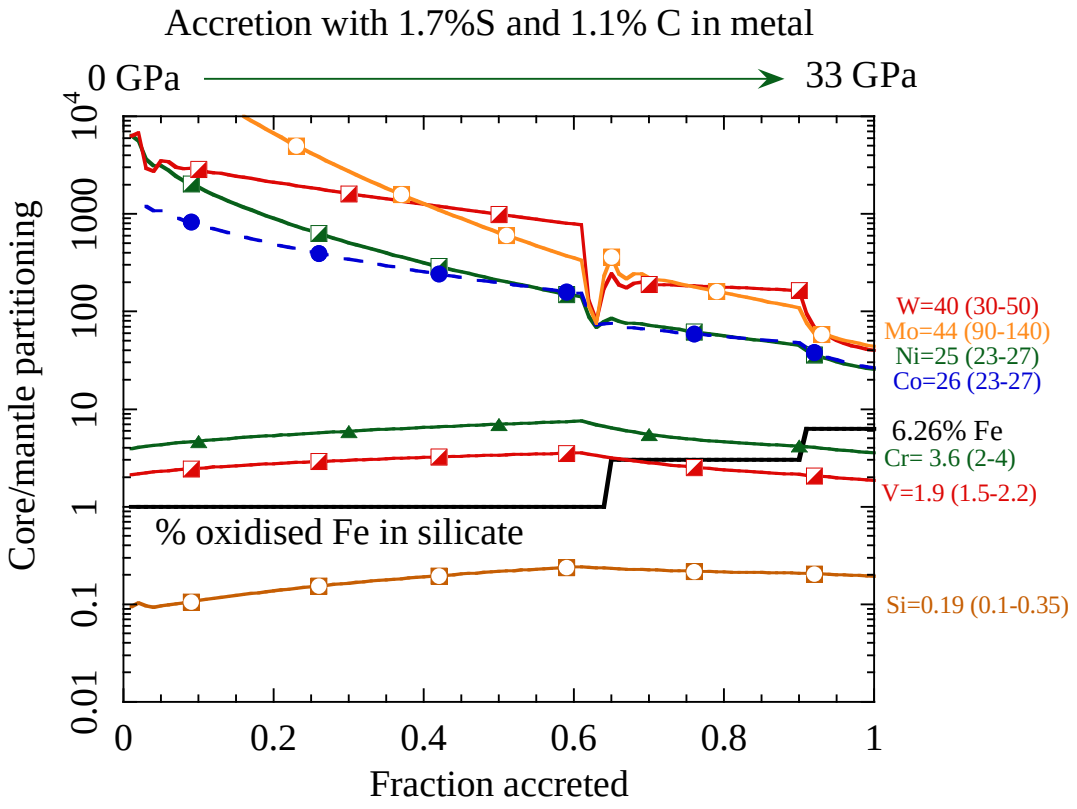

Fig. 8. Continuous accretion model with 1.7%S and 1.1%C, which reproduces the estimated core–mantle partitioning behaviour of Table 7. Epsilon-parameters for the metal derived in this study were used.

Schönbächler *et al.* (2010) used the isotopic composition of moderately volatile Ag in silicate Earth to argue that the Pd/Ag ratio of the material which delivered Ag to the Earth was approximately chondritic and had remained chondritic during the lifetime of ^{107}Pd (half-life= 6.5 Myr decay to ^{107}Ag). Since the earth accreted, according to Hf-W chronometry in about 30 Myr (Yin *et al.* 2002) the requirement of accretion of Pd/Ag with chondritic ratio means that Ag was not accreted to Earth until near the end of that period. Otherwise, because Pd/Ag of

silicate Earth is subchondritic the $^{107}Ag/^{109}Ag$ of silicate Earth would also be subchondritic. To be consistent with this finding the accretion of S (1.7% S in the core) and C (1.1%C in the core) to the Earth was therefore assumed to take place in the last 10-20% of growth of the Earth. As can be seen from Fig 9, this model has a dramatic effect on Mo/W and on total Mo partitioning between core and mantle. It is, as can be seen, now possible to match the required partitioning of Mo between core and mantle to that required, while maintaining agreement with the expected for partitioning for the other refractory elements.

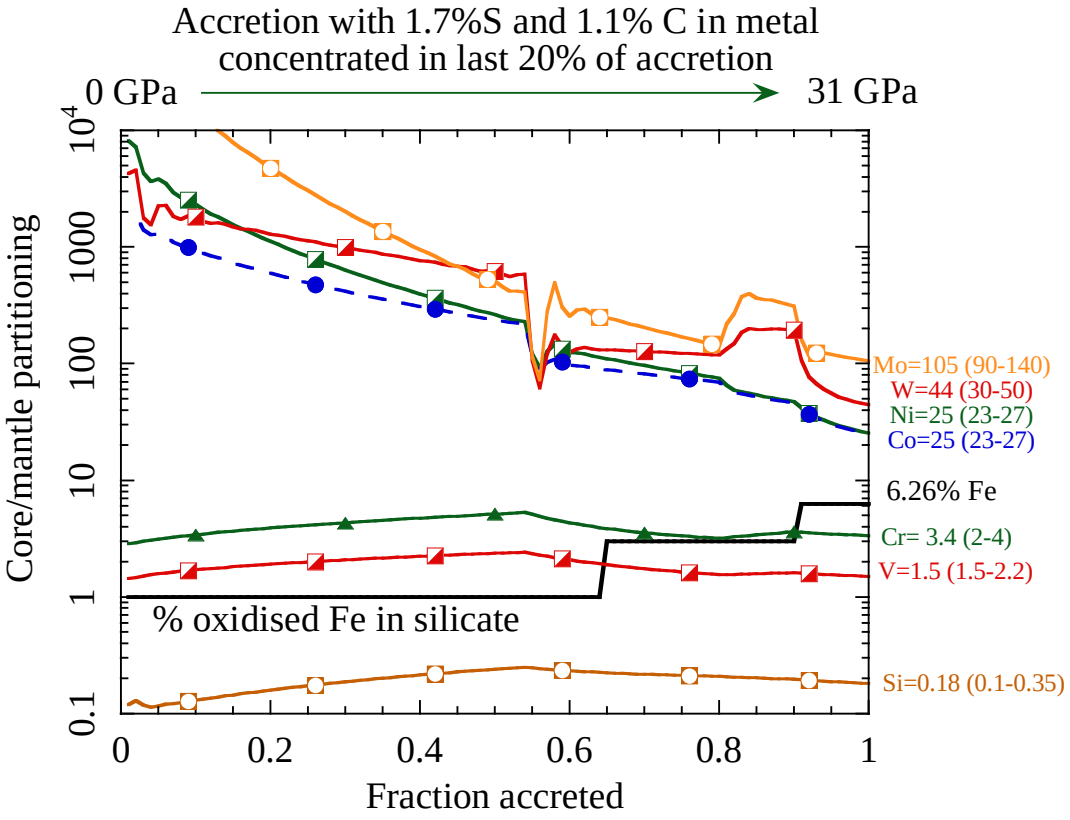

Fig. 9. Continuous accretion model considering that the accretion of S (1.7% S in the core) and C (1.1%C in the core) to the Earth took place in the last 10-20% of growth of the Earth. Epsilon-parameters for the metal derived in this study were used.

This shows that the Mo/W ratio of silicate Earth can only be reproduced by a model in which the S and C contents of the core were accreted during the last ~20% of accretion.

Chapter 5. Conclusions

- In this thesis I experimentally determined the effect of carbon on partitioning of Ni, Co, Mo and W between silicate and sulphide liquids and the effect of sulphur on partitioning of Ni, Co, Mo, W, Cu, Mn, Ag, Sb, Cd, In, Tl, Pb, Ga, Ge, Cr, V and Zn;
- Ni and Co become less siderophile with increasing S and C content (from 200 and 30 at 0% S to 50 and 15 at 36% S, respectively). Meanwhile Mo and W become less siderophile given increasing S, (from 13 and 0.01 at 0% S to 0.75 and $9x10^{-6}$ at 36% S, respectively), but in the presence of increasing C become more siderophile (from 10 and 0.01 at 0% C to 50/90 and 0.08/0.1 at 5.5% C, respectively). Ni is an order of magnitude greater than Co and Mo more that three orders of magnitude greater than W in K_D values;
- The calculated epsilon values accounting for the effect of sulphur on metal-silicate partitioning are the following; ε^S_{Ni}: 2.11 (±0.19), ε^S_{Co}: 2.33 (±0.27), ε^S_{Mo}: 4.73 (±1.55), ε^S_{W}: 12.16 (±2.87), ε^S_{Cu}: -2.12±0.33), ε^S_{Mn}: -6.57±0.59), ε^S_{V}: -3.32±0.33), ε^S_{Ge}: 7.37 (±1.35), ε^S_{Cr}: -3.39 (±0.17) and ε^S_{Pb}: -3.45 (±0.27).
- These values have been incorporated into an accretion model that integrated the Si partition coefficient equation of Tuff *et al* (2011) and the oxygen solubility model of Ozawa *et al* (2008).
- According to the model, the Mo/W ratio of silicate Earth can only be reproduced by a model in which the S and C contents of the core were accreted during the last ~20% of accretion;
- The best model which fit everything including the Mo: W ratio of the silicate Earth involved the Earth accreting in steps of increasing oxidation from 1 to 6.26% FeO, increasing Si content of the core and the light

elements C and S being added to the Earth in the last 20% of accreting material.

Bibliography

Albarede, F., 2009. Volatile accretion history of the terrestrial planets and dynamic implications. Nature 461, 1227-1233.

Allegre, C.J., Poirier, J.P., Humler, E., Hofmann, A.W., 1995. The Chemical-Composition of the Earth. Earth Planetary Science Letters 134, 515-526.

Allegre, C.J., Manhes, G., Lewin, E., 2001. Chemical composition of the Earth and the volatility control on planetary genetics. Earth Planetary Science Letters 185, 1-2, 49-69.

Asahara, Y., Frost, D.J., Rubie, D.C., 2007. Partitioning of FeO between magnesiowustite and liquid iron at high pressures and temperatures: Implications for the composition of the Earth's outer core. Earth Planetary Science Letters 257, 435-449.

Azbel, I.Y., Tolstikhin, I.N., Kramers, J.D., Pechernikova, G.V., Vityazev, A.V., 1993. Core growth and siderophile element depletion of the mantle during homogeneous Earth accretion. Geochimica et Cosmochimica Acta 57, 2889-2898.

Baker, J., Bizzarro, M., Wittig, N., Connelly, J., Haack, H., 2005. Early planetesimal melting from an age of 4.5662 Gyr for differentiated meteorites. Nature 436, 1127-1131.

Christiansen, Eric H., 1995. Exploring the Planets, 2nd Edition, New York: Prentice Hall.

Corgne, A., Siebert, J., Badro, J., 2009. Oxygen as a light element: A solution to single-stage core formation. Earth Planetary Science Letters 288, 108-114.

Cottrell, E., Walter, M.J., Walker, D., 2009. Metal-silicate partitioning of tungsten at high pressure and temperature: Implications for equilibrium core formation in Earth. Earth Planetary Science Letters 281, 275-287.

Dreibus, G., Jagoutz, E., Palme, H., Spettel, B., Wanke, H., 1979. Volatile and other trace-element abundances in the eucrite parent body and in the Earth's mantle - comparison. Meteoritics 14, 385-387.

Dreibus, G., Palme, H., 1996. Cosmochemical constraints on the sulfur content in the Earth's core. Geochimica et Cosmochimica Acta 60, 1125-1130.

Ertel, W., Walter, M.J., Drake, M.J., Sylvester, P.J., 2006. Experimental study of platinum solubility in silicate melt to 14 GPa and 2273 K: Implications for accretion and core formation in Earth. Geochimica et Cosmochimica Acta 70, 2591-2602.

Georg, R.B., Halliday, A.N., Schauble, E.A., Reynolds, B.C., 2007. Silicon in the Earth's core. Nature 447, 1102-1106.

Halliday, A., Rehkamper, M., Lee, D.C., Yi, W, 1996. Early evolution of the Earth and Moon: New constraints from Hf-W isotope geochronometry. Earth Planetary Science Letters, 142, 1-2, 75-89.

Jana, D., Walker, D., 1997. The impact of carbon on element distribution during core formation. Geochimica et Cosmochimica Acta 61, 2759-2763.

Kegler, P., Holzheid, A., Frost, D.J., Rubie, D.C., Dohmen, R., Palme, H., 2008. New Ni and Co metal-silicate partitioning data and their relevance for an early terrestrial magma ocean. Earth Planetary Science Letters 268, 28-40.

Kokubo, E., Ida, S., 2000. Formation of protoplanets from planetesimals in the solar nebula. Icarus 143, 15-27.

König, S., Münker, C., Hohl, S., Paulick, H., Barth, AR., Lagos, M., Pfänder, J., Büchl, A., 2011. The Earth's tungsten budget during mantle melting and crust formation. Geochimica et Cosmochimica Acta 75:2119-2136

Li, J., Agee, C.B., 1996. Geochemistry of mantle-core differentiation at high pressure. Nature 381, 686-689.

Li, J., Agee, C.B., 2001. Element partitioning constraints on the light element composition of the Earth's core. Geophysical Research Letters 28, 81-84.

Ma, Z.T., 2001. Thermodynamic description for concentrated metallic solutions using interaction parameters. Metallurgical and Materials Transactions B-Process Metallurgy and Materials Processing Science Vol. 32, 1, 87-103.

Mann, U., Frost, D.J., Rubie, D.C., 2009. Evidence for high-pressure core-mantle differentiation from the metal-silicate partitioning of lithophile and weakly-siderophile elements. Geochimica et Cosmochimica Acta 73, 7360-7386.

McDonough, W.F., Sun, S.S., 1995. The Composition Of The Earth. Chemical Geology 120, 223-253.

Mcqueen, R.G., Marsh, S.P., 1966. Shock-wave compression of iron-nickel alloys and Earth's core. Journal of Geophysical Research 71, 6, 1751-1756.

O'Neill, H.S.C., 1991. The origin of the moon and the early history of the Earth—A chemical model. Part 1: The Moon. Geochimica et Cosmochimica Acta 55, 1135-1157.

O'Neill HSC, Eggins SM, 2002. The effect of melt composition on trace element partitioning: an experimental investigation of the activity coefficients of FeO, NiO, CoO, MoO_2 and MoO_3 in silicate melts. Chemical Geology 186(1-2):151-181.

Ono-Nakazato, H., Taguchi, K., Maruo, R., Usui, T., 2007. Silicon deoxidation equilibrium of molten Fe-Mo alloy. Isij Int 47, 365-369.

Ozawa, H., Hirose, K., Mitome, M., Bando, Y., Sata, N., Ohishi, Y., 2008. Chemical equilibrium between ferropericlase and molten iron to 134 GPa and implications for iron content at the bottom of the mantle. Geophysical Research Letters. 35.

Peale, S. J., Cassen, P. & Reynolds, R. T., 1979. Melting of Io by tidal dissipation. American Association for the Advancement of Science, Vol. 203, No. 4383, pp. 892-894

Presnall, D.C., Dixon, S.A., Dixon, J.R., Odonnell, T.H., Brenner, N.L., Schrock, R.L., Dycus, D.W., 1978. Liquidus phase relations on join diopside-forsterite-anorthite from 1 Atm to 20 kbar - Their bearing on generation and crystallization of basaltic magma. Contributions to Mineralogy and Petrology 66, 203-220.

Righter, K., 2011. Prediction of metal-silicate partition coefficients for siderophile elements: An update and assessment of PT conditions for metal-silicate equilibrium during accretion of the Earth. Earth Planetary Science Letters 304, 158-167.

Righter, K., Drake, M.J., 1996. Core formation in Earth's moon, Mars, and Vesta. Icarus 124, 513-529.

Ringwood, A.E., 1966. Chemical evolution of terrestrial planets. Geochimica et Cosmochimica Acta 30, 41-&.

Rubie, D.C., Gessmann, C.K., Frost, D.J., 2004. Partitioning of oxygen during core formation on the Earth and Mars. Nature 429, 58-61.

Schönbächler, M., Carlson, R.W., Horan, M.F., Mock, T.D., Hauri, E.H., 2010. Heterogeneous accretion and the moderately volatile element budget of Earth. Science 328, 884-887.

Shahar, A., Ziegler, K., Young, E.D., Ricolleau, A., Schauble, E.A., Fei, Y.W., 2009. Experimentally determined Si isotope fractionation between silicate and Fe metal and implications for Earth's core formation. Earth Planetary Science Letters 288, 228-234.

Siebert, J., Corgne, A., Ryerson, F.J., 2011. Systematics of metal-silicate partitioning for many siderophile elements applied to Earth's core formation. Geochimica et Cosmochimica Acta 75, 1451-1489.

Steelmaking JSftPoSattCo,1988. Steelmaking Data Sourcebook. Gordon and Breach, New York

Stevenson DJ,1981. Models of the Earth's core. Science 214:611-619

Thibault, Y., Walter, M.J., 1995. The influence of pressure and temperature on the metal-silicate partition-coefficients of nickel and cobalt in a Model-C1 chondrite and implications for metal segregation in a deep magma ocean. Geochimica et Cosmochimica Acta 59, 991-1002.

Tronnes, R.G., Frost, D.J., 2002. Peridotite melting and mineral-melt partitioning of major and minor elements at 22-24.5 GPa. Earth Planetary Science Letters 197, 117-131.

Tuff, J., Wood, B.J., Wade, J., 2011. The effect of Si on metal-silicate partitioning of siderophile elements and implications for the conditions of core formation. Geochimica et Cosmochimica Acta 75, 673-690.

Wade, J., Wood, B.J., 2005. Core formation and the oxidation state of the Earth. Earth Planetary Science Letters 236, 78-95.

Wade, J., Wood, B.J., 2012. Metal-silicate partitioning experiments in the diamond anvil cell: A comment on potential analytical errors. Physics of the Earth and Planetary Interiors 192, 54-58.

Walker, R.J., 2009. Highly siderophile elements in the Earth, Moon and Mars: Update and implications for planetary accretion and differentiation. Chemie Der Erde-Geochemistry. 69, 101-125.

Wänke, H., 1981. Constitution of terrestrial planets. Philosophical Transactions of the Royal Society 303, 287-302.

Wood, B.J., 1993. Carbon in the Core. Earth Planetary Science Letters 117, 593-607.

Wood, B.J., Halliday, A.N., 2010. The lead isotopic age of the Earth can be explained by core formation alone. Nature 465, 767-U764.

Wood, B.J., Wade, J., Kilburn, M.R., 2008. Core formation and the oxidation state of the Earth: Additional constraints from Nb, V and Cr partitioning. Geochimica et Cosmochimica Acta 72, 1415-1426.

Yin, Q.Z., Jacobsen, S.B., Yamashita, K., Blichert-Toft, J., Telouk, P., Albarede, F., 2002. A short timescale for terrestrial planet formation from Hf-W chronometry of meteorites. Nature 418, 949-952.

Zerr, A., Diegeler, A., Boehler, R., 1998. Solidus of Earth's deep mantle. Science 281, 243-246.

Zhang, J.Z., Herzberg, C., 1994. Melting experiments on anhydrous peridotite KLB-1 from 5.0 to 22.5 GPa. Journal of Geophysical Research Letters-Solid Earth 99, 17729-17742.

Appendices

Table 1. List of experimental runs and compositions.

Run №	Composition	T, °C	Capsule Type	Run time (minutes)
A312	50% CMAS + 50% Fe	1550	MgO	30
A314	30% CMAS + 70% FeS	1500	MgO	30
A319	30% CMAS + 70% FeS	1550	MgO	30
A315	30% CMAS + 55% FeS + 15% Fe	1550	MgO	30
A318	30% CMAS + 55% FeS + 15% Fe	1550	MgO	30
A316	30% CMAS + 35% FeS + 35% Fe	1550	MgO	30
A317	30% CMAS + 20% FeS + 50% Fe	1550	MgO	30
A321	30% CMAS + 50% FeS + 20% Fe	1550	MgO	30
A322	30% CMAS + 50% FeS + 20% Fe	1550	MgO	30
A232	25% CMAS + 75% Fe	1650	Si	20
A239	25% CMAS + 42.5%Fe + 7.5% FeS	1650	Si	20
A241	25% CMAS + 75% Fe	1650	Gr	20
A242	25% CMAS + 75% FeS	1650	Si	20
A243	23.75% CMAS + 1.25% FeO + 75% Fe	1650	Gr	20
A244	25% CMAS + 75% Fe	1650	Gr	20
A245	23.75% CMAS + 1.25% FeO + 75% Fe	1650	Gr	20
BW1210	45%CMAS+5%FeO+25%Fe+25%FeS	1650	MgO	33
BW1212	45%CMAS+5%FeO+10%Fe+40%FeS	1650	MgO	34
BW1214	25%CMAS+37%Fe+37%FeS	1650	MgO	20
BW1215	25%CMAS+75%Fe	1650	MgO	30
BW1216	25%CMAS+30%Fe+45%FeS	1650	MgO	30
BW1220	25%CMAS+50%Fe+25%FeS	1650	MgO	20

BW1046	40%CMAS+60%Fe		1650	MgO	42

Pressure - 1.5 GPa = 1200 psi in $BaCO_3$ sleeve + Si-glass assembly

Trace element mixture included: Ni, Co, Mo, W, Cu, Ag, Tl, In, Cr, Mn, V, Ga, Ge, Cd, Sb, Zn

Table 2. Major element composition of silicate glasses

Run №	**A312**	**σ**	**A314**	**σ**	**A319**	**σ**	**A315**	**σ**
MgO	20.27	0.63	19.51	0.15	20.27	0.09	22.54	0.96
Al_2O_3	14.72	0.34	16.60	0.35	15.46	0.07	15.05	0.56
SiO_2	42.22	0.18	44.72	0.27	43.18	0.16	42.00	0.30
SO_3	_	_	1.30	0.13	1.66	0.19	1.58	0.15
CaO	20.70	0.39	17.47	0.19	17.94	0.08	19.25	0.59
FeO	2.22	0.04	1.65	0.10	1.50	0.15	1.55	0.13
Totals	100.24		101.34		100.11		102.08	

Run №	**A318**	**σ**	**A316**	**σ**	**A317**	**σ**	**A321**	**σ**
MgO	19.48	0.23	19.50	1.08	19.32	0.43	22.21	0.33
Al_2O_3	14.71	0.09	13.90	0.31	12.83	0.07	14.15	0.16
SiO_2	42.32	0.13	40.43	0.18	40.82	0.14	42.22	0.33
SO_3	1.46	0.14	0.20	0.03	_	_	0.44	0.02
CaO	20.76	0.18	21.59	0.77	22.30	0.26	19.99	0.24
FeO	1.27	0.12	1.69	0.04	3.14	0.05	2.20	0.05
Totals	100.12		97.45		98.63		101.32	

(continued)

Run №	A322	A232	σ	A239	σ	A241	σ
MgO	21.71	11.46	0.06	10.24	0.06	15.89	0.09
Al_2O_3	14.21	9.72	0.10	7.44	0.07	16.51	0.15
SiO_2	42.11	63.43	0.13	60.83	0.26	42.18	0.21
SO_3	0.59	–	–	–	–	–	–
CaO	19.85	8.11	0.05	7.05	0.04	15.81	0.05
FeO	2.09	7.32	0.10	14.39	0.11	10.39	0.08
Totals	100.68	100.05		99.95		100.78	

Run №	A242	σ	A243	σ	A244	σ	A245	σ
MgO	21.19	0.15	15.07	0.07	15.68	0.11	14.51	0.16
Al_2O_3	7.02	0.06	15.59	0.08	14.89	0.15	15.82	0.17
SiO_2	65.71	0.27	39.55	0.13	38.20	0.23	39.24	0.35
SO_3	–	–	–	–	–	–	–	–
CaO	5.68	0.03	15.08	0.05	14.62	0.05	14.95	0.10
FeO	1.80	0.18	14.59	0.11	15.24	0.15	15.58	0.18
Totals	101.39		99.87		98.62		100.10	

(continued)

Run №	BW1210	σ	BW1212	σ	BW1214	σ	BW1215	σ
MgO	27.50	9.23	20.26	3.45	30.40	9.87	26.19	6.68
Al_2O_3	13.54	3.83	17.27	0.64	13.48	4.32	12.03	2.50
SiO_2	37.76	1.03	30.93	1.04	32.91	3.07	35.34	1.13
SO_3	–	–	–	–	–	–	–	–
CaO	15.70	5.30	22.56	2.35	15.75	6.14	15.93	3.91
FeO	6.22	0.56	7.23	0.73	7.80	1.89	10.27	0.78
Totals	100.71		98.26		100.34		99.77	

Run №	BW1216	σ	BW1220	σ	BW1046	σ
MgO	27.16	9.41	12.91	0.23	16.62	0.25
Al_2O_3	12.30	3.49	8.76	0.06	8.64	0.14
SiO_2	35.86	1.59	66.08	0.40	63.11	0.08
SO_3	–	–	–	–	–	–
CaO	16.60	5.56	7.72	0.11	8.64	0.14
FeO	7.08	0.88	5.39	0.18	3.61	0.10
Totals	99.00		100.86		100.62	

Table 3: Major element composition of sulphides

Run №	A312	σ	A314	σ	A319	σ	A315	σ
W%(O)	_	_	0.26	0.08	0.31	0.07	0.13	0.09
W%(S)	0.09	0.16	37.80	0.29	37.84	0.34	30.60	0.74
W%(Fe)	96.92	0.49	60.88	0.39	60.88	0.40	69.95	0.85
W%(Ni)	0.66	0.04	0.13	0.02	0.13	0.03	0.05	0.02
W%(Cu)	0.39	0.03	0.08	0.03	0.10	0.02	0.07	0.03
W%(Mo)	_	_	_	_	_	_	_	_
W%(W)	_	_	_	_	_	_	_	_
W%(C)	_	_	_	_	_	_	_	_
Totals	98.14		99.16		99.25		100.79	

Run №	A318	σ	A316	σ	A317	σ	A321	σ
W%(O)	0.51	0.14	0.19	0.03	0.11	0.02	_	_
W%(S)	28.75	4.65	1.52	0.34	0.46	0.59	4.58	0.21
W%(Fe)	70.72	4.02	97.41	0.48	97.96	0.70	92.62	0.20
W%(Ni)	_	_	_	_	0.35	0.03	_	_
W%(Cu)	_	_	_	_	_	_	_	_
W%(Mo)	_	_	_	_	_	_	_	_
W%(W)	_	_	_	_	_	_	_	_
W%(C)	_	_	_	_	_	_	_	_
Totals	100.13		99.18		98.95		97.37	

(continued)

Run №	A322	σ	A232	σ	A239	σ	A241	σ
W%(O)	_	_	_	_	_	_	_	_
W%(S)	6.50	0.68	_	_	2.44	0.70	_	_
W%(Fe)	90.32	0.67	97.14	0.46	95.82	0.95	92.08	0.40
W%(Ni)	_	_	1.61	0.05	1.21	0.04	1.38	0.13
W%(Cu)	0.11	0.03	_	_	_	_	_	_
W%(Mo)	_	_	_	_	_	_	_	_
W%(W)	_	_	_	_	_	_	_	_
W%(C)	_	_	_	_	_	_	_	_
Totals	97.06		98.75		99.47		98.96	

Run №	A242	σ	A243	σ	A244	σ	A245	σ
W%(O)	_	_	_	_	_	_	_	_
W%(S)	36.26	1.01	_	_	_	_	_	_
W%(Fe)	61.12	0.40	92.78	0.68	91.51	0.78	91.56	0.90
W%(Ni)	1.32	0.48	1.10	0.06	_	_	_	_
W%(Cu)	_	_	_	_	_	_	_	_
W%(Mo)	_	_	_	_	0.99	0.21	1.13	0.13
W%(W)	_	_	_	_	1.19	0.24	1.53	0.17
W%(C)	_	_	5.50	_	5.50	_	5.50	_
Totals	98.70		99.38		99.19		99.72	

(continued)

Run №	BW1210	σ	BW1212	σ	BW1214	σ	BW1215	σ
W%(O)	_	_	_	_	0.29	0.13	_	_
W%(S)	4.60	0.37	31.12	2.08	3.01	0.64	_	_
W%(Fe)	91.26	0.45	64.65	2.02	90.65	0.69	96.12	0.40
W%(Ni)	_	_	_	_	_	_	_	_
W%(Cu)	_	_	_	_	_	_	_	_
W%(Mo)	2.57	0.05			2.24	0.08	2.03	0.04
W%(W)	1.76	0.05	0.47	0.10	4.00	0.11	1.09	0.03
W%(C)	_	_	_	_	_	_	_	_
Totals	100.19		96.24		100.19		99.24	

Run №	BW1216	σ	BW1220	σ	BW1046	σ
W%(O)	1.04	0.37	_	_	_	_
W%(S)	22.15	2.98	13.45	2.27	_	_
W%(Fe)	74.32	3.24	84.47	2.13	87.18	0.27
W%(Ni)	_	_	1.42	0.13	6.55	0.04
W%(Cu)	_	_	_	_	_	_
W%(Mo)	0.59	0.12	_	_	_	_
W%(W)	0.50	0.17	_	_	_	_
W%(C)	_	_	_	_	_	_
Totals	98.60		99.34		93.73	

Table 4. Trace element composition of silicate glasses

Run №	A312	σ	A314	σ	A319	σ	A315	σ
Cu65	26.57	1.75	1.47	0.41	1.90	0.25	2.72	0.40
Ga71	16.85	0.34	743.13	20.29	649.77	6.84	67.48	2.44
Ge74	0.57	0.13	186.59	10.19	178.14	19.46	0.63	0.13
Ag107	32.23	0.46	0.60	0.12	1.36	0.14	0.32	0.05
Sb121	0.49	0.17	2.69	0.49	3.44	0.40	0.10	0.00
Ti47	60.55	2.19	58.33	1.62	66.85	1.77	61.25	2.28
V51	626.77	12.45	410.04	17.18	508.33	57.78	114.35	8.47
Mn55	63.11	0.97	98.23	1.00	84.77	1.61	219.60	4.69
Co59	–	–	–	–	–	–	–	–
Zn66	379.64	6.75	51.75	1.97	43.88	1.42	44.81	2.15
Cd111	3.38	0.37	1.75	0.30	3.00	0.22	0.70	0.19
In115	135.25	2.17	4.63	0.58	9.80	0.31	2.20	0.09
Tl205	917.22	10.00	12.05	1.19	23.96	1.37	11.88	0.31
Pb208	130.52	2.33	4.32	0.65	8.48	0.61	0.74	0.09
Cr53	494.89	10.32	144.14	35.32	164.68	12.99	106.22	3.97
Ni60	3.97	0.18	0.71	0.10	0.53	0.16	0.72	0.07
Mo	–	–	–	–	–	–	–	–
W	–	–	–	–	–	–	–	–

(continued)

Run №	A318	σ	A316	σ	A317	σ	A321	σ
Cu65	2.62	0.60	2.20	0.26	5.70	0.31	7.19	0.82
Ga71	105.69	5.31	15.51	1.09	54.19	2.48	156.98	24.07
Ge74	1.36	0.57	0.37	0.03	0.41	0.03	_	_
Ag107	0.73	0.10	0.39	0.04	2.10	0.21	2.22	0.09
Sb121	0.12	0.06	0.05	0.01	0.06	0.01	_	_
Ti47	71.53	1.46	61.94	3.03	78.29	1.35	59.11	2.76
V51	123.32	12.34	754.47	17.19	1409.15	38.87	1632.85	24.18
Mn55	241.79	6.60	273.27	11.22	260.45	3.62	342.81	4.25
Co59	_	_	_	_	_	_	_	_
Zn66	53.72	3.44	113.09	5.93	546.23	26.85	335.20	17.08
Cd111	0.94	0.23	1.66	0.17	15.52	1.27	8.91	0.65
In115	3.94	0.31	1.00	0.08	3.99	0.34	_	_
Tl205	20.67	1.30	39.06	2.51	127.47	9.27	98.27	2.39
Pb208	1.56	0.26	0.85	0.08	5.91	0.45	5.06	0.83
Cr53	152.80	26.26	622.49	12.15	1035.34	34.87	1509.82	23.28
Ni60	0.55	0.15	0.39	0.03	0.60	0.11	2.91	1.92
Mo	_	_	_	_	_	_	_	_
W	_	_	_	_	_	_	_	_

(continued)

Run №	A322	σ	A232	σ	A239	σ	A241	σ
Cu65	8.26	0.87	_	_	_	_	_	_
Ga71	205.93	14.95	_	_	_	_	_	_
Ge74	_	_	_	_	_	_	_	_
Ag107	3.68	0.59	_	_	_	_	_	_
Sb121	_	_	_	_	_	_	_	_
Ti47	59.21	0.61	_	_	_	_	_	_
V51	1728.72	355.03	_	_	_	_	_	_
Mn55	362.11	2.40	_	_	_	_	_	_
Co59	_	_	23.46	0.79	41.42	0.94	54.89	1.05
Zn66	400.27	51.87	_	_	_	_	_	_
Cd111	14.52	0.65	_	_	_	_	_	_
In115	_	_	_	_	_	_	_	_
Tl205	91.46	3.55	_	_	_	_	_	_
Pb208	5.21	0.22	_	_	_	_	_	_
Cr53	1577.58	476.44	_	_	_	_	_	_
Ni60	1.37	0.55	5.36	0.50	8.02	0.62	13.77	0.70
Mo	_	_	_	_	_	_	_	_
W	_	_	_	_	_	_	_	_

(continued)

Run №	A242	σ	A243	σ	A244	σ	A245	σ
Cu65	–	–	–	–	–	–	–	–
Ga71	–	–	–	–	–	–	–	–
Ge74	–	–	–	–	–	–	–	–
Ag107	–	–	–	–	–	–	–	–
Sb121	–	–	–	–	–	–	–	–
Ti47	–	–	–	–	–	–	–	–
V51	–	–	–	–	–	–	–	–
Mn55	–	–	–	–	–	–	–	–
Co59	42.24	1.21	88.78	8.39	–	–	–	–
Zn66	–	–	–	–	–	–	–	–
Cd111	–	–	–	–	–	–	–	–
In115	–	–	–	–	–	–	–	–
Tl205	–	–	–	–	–	–	–	–
Pb208	–	–	–	–	–	–	–	–
Cr53	–	–	–	–	–	–	–	–
Ni60	7.06	0.35	17.04	1.50	–	–	–	–
Mo	–	–	–	–	2.96	0.42	2.29	0.30
W	–	–	–	–	260.39	8.16	424.37	63.21

(continued)

Run №	BW1210	σ	BW1212	σ	BW1214	σ	BW1215	σ
Cu65	–	–	–	–	–	–	–	–
Ga71	–	–	–	–	–	–	–	–
Ge74	–	–	–	–	–	–	–	–
Ag107	–	–	–	–	–	–	–	–
Sb121	–	–	–	–	–	–	–	–
Ti47	–	–	–	–	–	–	–	–
V51	–	–	–	–	–	–	–	–
Mn55	–	–	–	–	–	–	–	–
Co59	–	–	–	–	–	–	–	–
Zn66	–	–	–	–	–	–	–	–
Cd111	–	–	–	–	–	–	–	–
In115	–	–	–	–	–	–	–	–
Tl205	–	–	–	–	–	–	–	–
Pb208	–	–	–	–	–	–	–	–
Cr53	–	–	–	–	–	–	–	–
Ni60	–	–	–	–	–	–	–	–
Mo	3.62	0.41	63.81	10.20	13.10	1.50	18.84	2.84
W	247.29	4.43	7477.69	844.55	2326.00	275.00	631.24	25.59

(continued)

Run №	BW1216	σ	BW1220	σ	BW1046	σ
Cu65	–	–	–	–	–	–
Ga71	–	–	–	–	–	–
Ge74	–	–	–	–	–	–
Ag107	–	–	–	–	–	–
Sb121	–	–	–	–	–	–
Ti47	–	–	–	–	–	–
V51	–	–	–	–	–	–
Mn55	–	–	–	–	–	–
Co59	–	–	22.36	0.41	39.20	0.80
Zn66	–	–	–	–	–	–
Cd111	–	–	–	–	–	–
In115	–	–	–	–	–	–
Tl205	–	–	–	–	–	–
Pb208	–	–	–	–	–	–
Cr53	–	–	–	–	–	–
Ni60			5.14	0.41	9.76	0.85
Mo	5.80	1.64	–	–	–	–
W	1430.32	98.54	–	–	–	–

Table 5. Trace element composition of sulphides

Run №	A312	σ	A314	σ	A319	σ	A315	σ
Cu65	4225.26	167.80	759.24	32.78	655.77	62.19	590.28	50.52
Ga71	1381.30	50.69	554.04	37.95	561.02	33.20	361.32	71.77
Ge74	1419.25	55.22	2020.04	261.52	1916.67	84.95	219.66	68.23
Ag107	3117.91	363.56	319.74	27.92	1103.00	245.20	126.90	7.73
Sb121	5006.25	541.07	355.85	38.11	881.53	129.73	159.63	5.80
Ti47	3.77	0.45	2.03	0.13	1.68	0.52	1.72	0.08
V51	177.49	9.27	1180.39	37.80	1589.46	176.97	442.87	72.46
Mn55	3.79	1.86	376.79	13.46	365.87	13.75	233.59	23.03
Co59	_	_	_	_	_	_	_	_
Zn66	1586.07	125.00	625.60	37.17	543.33	15.24	253.09	24.47
Cd111	73.74	6.88	330.14	36.43	678.42	93.81	128.36	11.19
In115	8684.54	1009.75	340.84	24.89	865.68	116.39	192.05	13.22
Tl205	1161.43	158.30	630.95	82.42	1394.38	122.61	232.74	21.28
Pb208	3800.17	551.26	720.88	84.18	2401.63	747.19	147.73	14.06
Cr53	483.91	19.94	1926.09	56.75	2405.50	159.22	852.39	63.04
Ni60	_	_	_	_	_	_	_	_
Mo95	_	_	_	_	_	_	_	_
W182	_	_	_	_	_	_	_	_

(continued)

Run №	A318	σ	A316	σ	A317	σ	A321	σ
Cu65	700.88	54.61	283.67	14.28	671.88	29.61	758.80	62.45
Ga71	328.79	87.37	2075.29	44.20	2418.72	60.29	7553.35	572.42
Ge74	217.43	116.40	2283.23	61.46	2675.11	83.58	8248.45	273.21
Ag107	331.32	15.26	27.45	1.07	125.58	19.46	140.65	11.79
Sb121	229.38	16.47	370.45	13.32	1501.95	152.87	524.97	18.72
Ti47	1.23	0.12	1.31	0.10	1.70	0.05	1.44	0.38
V51	618.22	50.67	434.21	17.82	212.84	20.22	675.98	54.08
Mn55	226.66	8.53	11.75	0.76	10.12	2.02	12.13	1.69
Co59	–	–	–	–	–	–	–	–
Zn66	268.24	13.98	536.02	35.33	1015.88	79.32	1051.70	141.02
Cd111	114.73	6.90	33.36	2.41	139.40	21.57	152.93	33.58
In115	421.67	38.82	52.50	2.57	151.58	22.04	180.11	17.06
Tl205	374.07	16.09	43.88	2.21	110.80	19.88	109.08	15.92
Pb208	402.87	35.11	27.83	0.93	104.47	19.16	114.51	12.16
Cr53	1183.62	53.43	931.07	28.16	671.23	37.42	1823.80	66.45
Ni60	–	–	–	–	–	–	–	–
Mo95	–	–	–	–	–	–	–	–
W182	–	–	–	–	–	–	–	–

(continued)

Run №	A322	σ	A232	σ	A239	σ	A241	σ
Cu65	816.06	9.19	_	_	_	_	_	_
Ga71	12824.13	456.79	_	_	_	_	_	_
Ge74	7533.13	71.98	_	_	_	_	_	_
Ag107	219.22	7.73	_	_	_	_	_	_
Sb121	642.54	17.92	_	_	_	_	_	_
Ti47	1.04	0.14	_	_	_	_	_	_
V51	715.17	29.55	_	_	_	_	_	_
Mn55	8.66	0.29	_	_	_	_	_	_
Co59	_	_	12157.00	66.00	9900.54	48.13	10162.65	65.61
Zn66	945.43	104.96	_	_	_	_	_	_
Cd111	239.81	37.35	_	_	_	_	_	_
In115	194.62	7.56	_	_	_	_	_	_
Tl205	120.77	5.80	_	_	_	_	_	_
Pb208	170.63	5.91	_	_	_	_	_	_
Cr53	1646.27	34.15	_	_	_	_	_	_
Ni60			16100.00	452.46	12100.38	385.89	13752.29	1255.41
Mo95	_	_	_	_	_	_	_	_
W182	_	_	_	_	_	_	_	_

(continued)

Run №	A242	σ	A243	σ	A244	σ	A245	σ
Cu65	–	–	–	–	–	–	–	–
Ga71	–	–	–	–	–	–	–	–
Ge74	–	–	–	–	–	–	–	–
Ag107	–	–	–	–	–	–	–	–
Sb121	–	–	–	–	–	–	–	–
Ti47	–	–	–	–	–	–	–	–
V51	–	–	–	–	–	–	–	–
Mn55	–	–	–	–	–	–	–	–
Co59	10435.00	258.00	10172.41	123.41	–	–	–	–
Zn66	–	–	–	–	–	–	–	–
Cd111	–	–	–	–	–	–	–	–
In115	–	–	–	–	–	–	–	–
Tl205	–	–	–	–	–	–	–	–
Pb208	–	–	–	–	–	–	–	–
Cr53	–	–	–	–	–	–	–	–
Ni60	13200.00	4800.00	10923.25	589.76	–	–	–	–
Mo95	–	–	–	–	–	–	–	–
W182	–	–	–	–	–	–	–	–

(continued)

Run №	BW1210	σ	BW1212	σ	BW1214	σ	BW1215	σ

Cu65	–	–	–	–	–	–	–	–
Ga71	–	–	–	–	–	–	–	–
Ge74	–	–	–	–	–	–	–	–
Ag107	–	–	–	–	–	–	–	–
Sb121	–	–	–	–	–	–	–	–
Ti47	–	–	–	–	–	–	–	–
V51	–	–	–	–	–	–	–	–
Mn55	–	–	–	–	–	–	–	–
Co59	–	–	–	–	–	–	–	–
Zn66	–	–	–	–	–	–	–	–
Cd111	–	–	–	–	–	–	–	–
In115	–	–	–	–	–	–	–	–
Tl205	–	–	–	–	–	–	–	–
Pb208	–	–	–	–	–	–	–	–
Cr53	–	–	–	–	–	–	–	–
Ni60	–	–	–	–	–	–	–	–
Mo95	–	–	5887.28	1223.95	–	–	–	–
W182	–	–	110.00	99.91	–	–	–	–

(continued)

Run <u>№</u>	**BW1216**	**σ**	**BW1220**	**σ**	**BW1046**	**σ**

Cu65	–	–	–	–	–	–
Ga71	–	–	–	–	–	–
Ge74	–	–	–	–	–	–
Ag107	–	–	–	–	–	–
Sb121	–	–	–	–	–	–
Ti47	–	–	–	–	–	–
V51	–	–	–	–	–	–
Mn55	–	–	–	–	–	–
Co59	–	–	10603.61	75.34	37000.00	40.00
Zn66	–	–	–	–	–	–
Cd111	–	–	–	–	–	–
In115	–	–	–	–	–	–
Tl205	–	–	–	–	–	–
Pb208	–	–	–	–	–	–
Cr53	–	–	–	–	–	–
Ni60	–	–	13988.04	1300.00	65500.00	40.00
Mo95	–	–	–	–	–	–
W182	–	–	–	–	–	–

Table 6. Equation parameters

	Constant	σ	Independent (ε)	σ	R^2
Ag	2.071	0.135	-3.788	0.311	0.948
Cd	-1.394	0.122	-3.902	0.280	0.960
Cr	-6.153	0.074	-3.391	0.170	0.980
Cu	2.681	0.142	-2.112	0.327	0.836
Ga	-1.476	0.157	6.632	0.36	0.977
Ge	-0.177	0.589	7.367	1.354	0.781
In	-2.271	0.132	-0.609	0.304	0.274
Mn	-7.571	0.259	-6.570	0.594	0.938
Pb	-0.872	0.116	-3.419	0.266	0.954
Sb	3.58	0.492	5.697	1.003	0.839
Tl	-2.176	0.102	-6.086	0.234	0.988
V	-7.229	0.144	-3.319	0.331	0.926
Zn	-3.002	0.181	-1.706	0.416	0.664
Ni	5.297	0.065	2.109	0.192	0.968
Co	3.475	0.091	2.333	0.272	0.948
Mo	2.616	0.518	4.728	1.553	0.674
W	-1.366	0.956	12.161	2.867	0.809

(continued)

For Carbon saturated experiments					
Ni	5.273	0.083	3.504	0.483	0.945
Co	3.413	0.054	2.865	0.313	0.965
Mo	2.018	0.154	-9.036	0.884	0.972
W	-2.354	0.174	-8.081	0.997	0.956

Table7. Partition coefficients consistent with Core – Mantle equilibration.

Element	McDonough & Sun (1995), McDonough (2003)	Allegre et al. (1995)	Likely range
D_V	1.83	—	1.5-2.2
D_{Fe}	13.66	13.65	13.65
D_{Si}	0.29	0.34	0.1-0.35*
D_{Cr}	3.4	2.9	2.0-4.0*
D_{Co}	23.8	24.7	23-27
D_{Ni}	26.5	24.4	23-27
D_{Nb}	—	—	0-0.8
D_W	(16)**	—	30-50
D_{Mo}	100	—	60-140

*Value uncertain due to volatility. ** New W content of silicate earth (König, *et al.* 2011)